Front. Earth Sci. 2022, 16(3): 711–733
https://doi.org/10.1007/s11707-021-0918-5

RESEARCH ARTICLE

Quantifying both climate and land use/cover changes on runoff variation in Han River basin, China

Jing TIAN[1], Shenglian GUO (✉)[1], Jiabo YIN[1], Zhengke PAN[2], Feng XIONG[3], Shaokun HE[1]

1 State Key Laboratory of Water Resources and Hydropower Engineering Science, Wuhan University, Wuhan 430072, China
2 Changjiang Institute of Survey, Planning, Design and Research, Wuhan 430010, China
3 Bureau of Hydrology, Changjiang Water Resources Commission, Wuhan 430010, China

Abstract Climate change and land use/cover change (LUCC) can both exert great impacts on the generation processes of precipitation and runoff. However, previous studies usually neglected considering the contribution component of future LUCC in evaluating changes in hydrological cycles. In this study, an integrated framework is developed to quantify and partition the impact of climate change and LUCC on future runoff evolution. First, a daily bias correction (DBC) method and the Cellular Automaton-Markov (CA-Markov) model are used to project future climate and LUCC scenarios, and then future runoff is simulated by the calibrated Soil and Water Assessment Tool (SWAT) model with different climate and LUCC scenarios. Finally, the uncertainty of future runoff and the contribution rate of the two driving factors are systematically quantified. The Han River basin in China was selected as a case study. Results indicate that: 1) both climate change and LUCC will contribute to future runoff intensification, the variation of future runoff under combined climate and LUCC is larger than these under climate change or LUCC alone; 2) the projected uncertainty of median value of multi-models under RCP4.5 (RCP8.5) will reach 18.14% (20.34%), 12.18% (14.71%), 11.01% (13.95%), and 11.41% (14.34%) at Baihe, Ankang, Danjiangkou, and Huangzhuang stations, respectively; 3) the contribution rate of climate change to runoff at Baihe, Ankang, Danjiangkou, and Huangzhuang stations under RCP4.5 (RCP8.5) are 91%–98% (84%–94%), while LUCC to runoff under RCP4.5 (RCP8.5) only accounts for 2%–9% (6%–16%) in the annual scale. This study may provide useful adaptive strategies for policy-makers on future water resources planning and management.

Received December 30, 2020; accepted June 3, 2021

E-mail: slguo@whu.edu.cn

Keywords climate change, LUCC, runoff response, uncertainty analysis, contribution rate

1 Introduction

Climate change and land use/cover change (LUCC) are the two main drivers that exert significant impacts on the generation processes of precipitation and runoff, which in turn alters the amount of water resources in the basin (Chen et al., 2007; Changnon and Gensini, 2019). Due to atmospheric warming, the moisture holding capacity of the atmosphere is increasing at a rate of 7% per degree centigrade (Yin et al., 2018). As a result, the mean and extreme precipitation in most parts of the world has increased significantly (Khazaei et al., 2012; Wu and Huang, 2004). LUCC can modify the underlying surface condition, which is essential for shaping runoff generation process and natural river flow regime (Costa et al., 2003; Mishra et al., 2012; Zuo et al., 2016; Umair et al., 2019). The soil water retention capacity may be impaired due to deforestation, which leads to increased rainfall-runoff rate and reduced soil infiltration. Hence, it is important to understand the potential mechanism between climate change/LUCC and the resulting impact in runoff (Schuol et al., 2008; Richey et al., 2015; Wang et al., 2017; Berihun et al., 2019; Clerici et al., 2019).

Recently, many studies have assessed the hydrological processes response to future climate change on at different scales (Kusangaya et al., 2014; Kundu et al., 2017; Yin et al., 2018). For instance, Chawla and Mujumdar (2015) used the VIC (Variable Infiltration Capacity) model to examine the runoff response in the upper Ganga basin. Lin et al. (2015) adopted the SWAT model to evaluate the impact of climate change on runoff of three catchments, and quantitatively compared the effects of different time scales (daily, annual and monthly scales) on runoff response. Yin et al. (2018) studied the effects of surface

temperature and atmospheric water content driven by natural and human activities on storm runoff extremes in a global scale. Shen et al. (2018) studied the impact of climate change on runoff in Han River basin, coupled the outputs of 20 GCMs under RCP4.5 and RCP8.5 with HMETS model. It was found that during 2020–2050, the average runoff under RCP4.5 will increase by 0.6% while that under RCP8.5 will decrease by 0.2%. Li et al. (2020) used a Budyko-based covariate analysis to evaluate the individual and combined effects of climate variability and human activities on streamflow in Han River basin. Results indicated that climate change was the dominant factor for streamflow decrease in the upper basin, while anthropogenic impact in the middle basin overweighed climate change. All the above studies show that climate change have substantial impacts on future runoff changes.

In addition, quantifying the uncertainty in the assessment of the impact of climate change on basin response is of great significance for scientific assessment of future climate disaster risk and guidance of future water resources planning and management. Generally, the uncertainty can be divided into five sources: global climate model (GCM), greenhouse gas emission scenario (GHGES), natural climate variability, downscaling method, and hydrological structure and parameters. A lot of studies (Zhang et al., 2011; Teng et al., 2012; Trolle et al., 2019) have been undertaken to quantify the uncertainty of the impact of climate change on the response of runoff from these sources. For example, Shen et al. (2018) employed 20 CMIP5 GCMs to show the climate and streamflow uncertainties in the upstream of Han River basin. Ahmadalipour et al. (2018) studied the uncertainties of climate model, downscaling method, and GHGES in the prediction of climate change in the Columbia River basin during 2020–2099. Previous studies have all shown that the selection of GCM is usually the biggest factor in the uncertainty of hydrological projections (Gu et al., 2020). Therefore, it is necessary to use multi-mode ensemble to assess the impact of climate change on runoff characteristics.

LUCC, caused by human activity, can alter runoff generation processes in complex ways. For instance, deforestation can influence the processes of runoff generation and concentration due to destruction of the safeguard provided by natural vegetation, resulting in soil erosion and ecosystem disorder, and then changing the surface harshness and infiltration rates. Rapid urbanization increases the area of impervious surface, which decreases the infiltration rate and time of concentration and thus resulting in runoff intensification (Lin et al., 2015; Umair et al., 2019). Several other human activities, such as agriculture irrigation, water transfer projects, and reservoir construction, can contribute to the soil moisture, and thus increasing runoff. To take such factors into consideration, most studies used historical LUCC and climate patterns as model input to investigate the runoff responses to different scenarios (Wagner et al., 2013; Chawla and Mujumdar, 2015;Yin et al., 2017). These studies focus on changes in water resources impacted by the projected climate variation while neglecting future LUCC evolution. As a result, the response of runoff to future LUCC has not been fully evaluated (Costa et al., 2003; Pan et al., 2017; Guo et al., 2020). As both climate change and LUCC have significant implications on future runoff and water resources (Tao et al., 2003; Yan et al., 2017; Woldesenbet et al., 2018), there is an urgent need to use the detection-and-attribution (D&A) framework to systematically detect climate change versus LUCC influence on the hydrological cycle and runoff generation. For example, Pan et al. (2017) generated future climate and LUCC scenarios predicted by the CA-Markov model, and used the SWAT model to estimate the runoff variation in the Beijiang River basin. Zhao et al. (2019) adopted the CA-Markov model to forecast LUCC which caused by ecological engineering, and used the InVEST model to calculate changes in carbon storage due to LUCC. Guo et al. (2020) used the CA-Markov model to simulate future LUCC scenarios of the Xinanjiang River basin, and appraised the combined impact of climate change and LUCC on streamflow under five GCMs and three RCPs scenarios. These assessment studies contribute to a better understanding on future water resources planning for ecological preservation and sustainable development.

However, some important problems have not been solved or discussed until now, such as: 1) how to make future LUCC simulation close to land use strategy and government planning? 2) How does the uncertainty of future runoff change with time? 3) How to quantify the contribution rate of the driving factors? The answers to these questions will provide a better understanding of how future climate change and LUCC impact runoff.

Therefore, the objectives of this paper are: 1) to make the future LUCC simulation close to land use strategy and government planning, and to systematically investigate the single and synthetic effects of future climate and LUCC on runoff; 2) to evaluate the uncertainty and the periodicity of future runoff; 3) to quantify the contribution rate of the two driving factors on future runoff. The remainder of this study is structured as follows: the methodology used in this study is shown in Section 2. The description of the case study is provided in Section 3. Section 4 shows the results, including the performances of the models, future climate and LUCC projection and runoff response. The detailed discussion is performed in Section 5 and our conclusions are summarized in Section 6.

2 Study area and data

2.1 Study area

The Han River basin is located at the largest tributary in the

middle reach of Yangtze River, with a drainage area of about 159000 km^2. The basin covers 20 prefectures (cities) and 78 counties (cities) in Hubei, Shaanxi, Sichuan, Chongqing, and Gansu regions. The subtropical monsoon climate and the changeable topography led to the spatiotemporal differences of the distribution of water resources. In the basin, the annual average temperature is 12°C–16°C, the general trend of annual precipitation is decreasing from southeast and southwest to northwest, the regional variation is between 800 and 1300 mm, and the runoff depth is between 300 and 900 mm. The sketch map of Han River basin, location of meteorological stations and hydrological stations are shown in Fig. 1.

There are obvious differences in the spatial distribution of LUCC types in the basin; the main types are forest land, farmland, and grassland, followed by construction land, water area, and bare land. A series of water conservancy projects have been built and distributed along the mainstream and tributaries of the Han River (Fig. 1). The Shiquan, Ankang, and Danjiangkou large-scale reservoirs have been built in the upper reach, while the cascade navigation projects have been carried out in the middle and lower reaches. The Yahekou, Shiquan, Danjiangkou, Huanglongtan, Ankang, Songshuling, Eping, Siping, Pankou, and Sanliping reservoirs were constructed in year of 1959, 1973, 1973, 1974, 1989, 2005, 2006, 2006, 2011, and 2011, respectively. As the boundary of the upper and mid-lower reaches of the Han River basin, the Danjiangkou reservoir is the water source of the middle route South-to-North Water Diversion Project, which fed water directly to the water receiving areas. This project focuses on solving the problem of water shortage in Henan, Hebei, Beijing, and Tianjin, and provide water for production, living, industry and agriculture. Therefore, it is very vital to quantify the impact of future climate change and future LUCC on hydrology in Han River basin, which will be very helpful for watershed managers to make future water transfer decisions.

2.2 Data

The DEM data at the spatial resolution of 90 m are provided by Geospatial Data Cloud, which is used to divide sub-basins for the SWAT model. The GCMs outputs include daily precipitation (prec), minimum temperature (T_{min}), maximum temperature (T_{max}), wind speed, solar radiation, and relative humidity of 25 meteorological stations. To represent possible model uncertainty, ten GCMs were selected in the Coupled Model Intercomparison Project Phase5 (CMIP5) of the Intergovernmental Panel on Climate Change (IPCC). The detailed information of the selected ten GCMs are presented in Table 1, and we use the data covering both historical (1966–2005) and future periods (2021–2060). RCPs include four scenarios in the CMIP5 framework: low emission (RCP2.6), medium emission (RCP4.5 and RCP6.0) and high emission (RCP8.5). The corresponding total radiation forcing stable in 2100 are about 2.6 W/m^2, 4.5 W/m^2, 6.0 W/m^2, and 8.5 W/m^2, respectively. In this study, both RCP4.5 and RCP8.5 are selected for research and analysis. Land use data with a spatial resolution of 1 km for LUCC1990, LUCC2000, LUCC2010 are derived

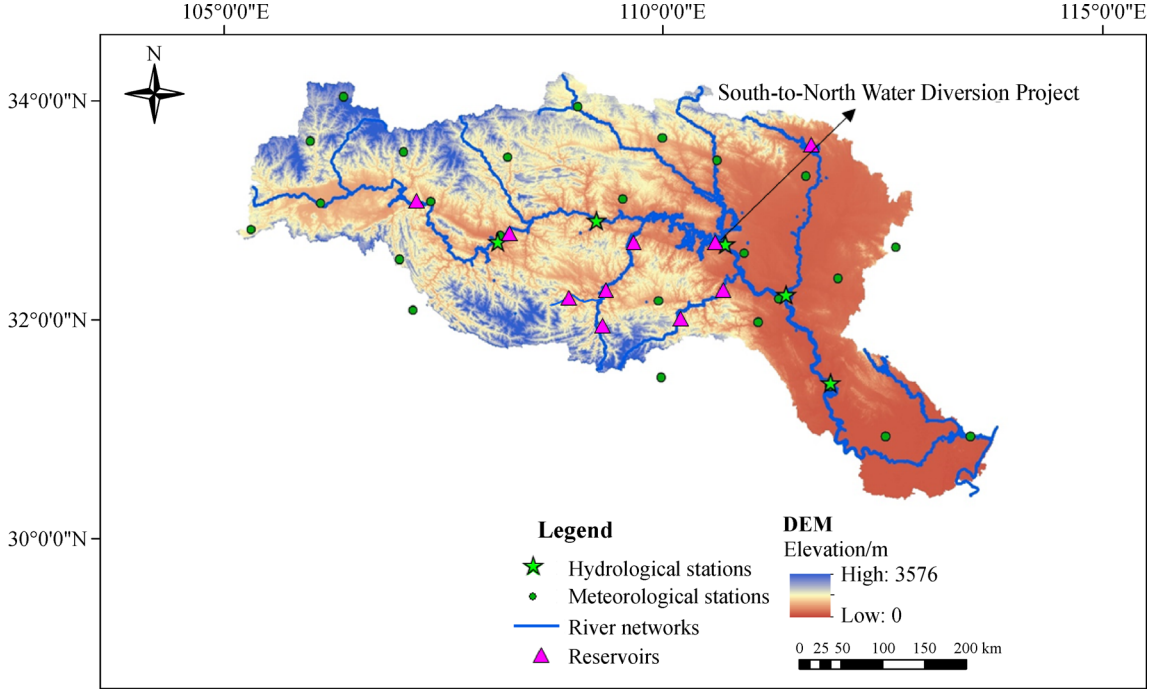

Fig. 1 Sketch image of the Han River basin.

Table 1 The basic information of the selected ten GCMs

ID	Model name	Institution	Resolution (Lon. ×Lat.)	Reference
G1	BCC-CSM1.1(m)	BCC, China	1.125°×1.125°	Wu (2012)
G2	BNU-ESM	GCESS, China	2.8°×2.8°	Ji et al. (2014)
G3	CanESM2	CCCMA, Canada	2.8°×2.8°	Yu et al. (2020)
G4	CCSM4	NCAR, USA	1.25°×0.94°	Silveira et al. (2019)
G5	CNRM-CM5	CNRM-CERFACS, Canada	1.4°×1.4°	Chauvin et al. (2017)
G6	CSIRO-Mk3.6.0	CSIRO-QCCCE, Australia	1.8°×1.8°	Zhang et al. (2017)
G7	GFDL-ESM2M	NOAA-GFDL, USA	2.5°×2.0°	Paymard et al. (2019)
G8	MRI-CGCM3	MRI, Japan	1.1°×1.1°	Zhang et al. (2019)
G9	MPI-ESM-LR	MPI-M, Germany	1.875°×1.875°	Block et al. (2013)
G10	NorESM1-M	NCC, Norway	2.5°×1.875°	Frey et al. (2021)

from the National Earth System Science Data Sharing Infrastructure, which is divided into the following six categories according to the standard of land resources remote sensing survey and classification: farmland, forestland, grassland, construction land, water body, and bare land. The soil data with a spatial resolution of 1 km is from Food and Agriculture Organization of the United Nations (FAO). Monthly runoff data at four (Ankang, Baihe, Danjiangkou, and Huangzhuang) hydrological stations in the mainstream of the Han River during 1980–2000 were collected at Yangtze River Water Conservancy Commission, which are used to calibrate the parameters of the hydrological model. Typical natural and socioeconomic indicators (including slope, elevation, distribution of road/railway/city and town, river network) are selected to compute transition potential maps of land use scenarios, which are obtained from Data Center for Resources and Environmental Sciences, Chinese Academy of Sciences.

3 Methods

Figure 2 shows the flowchart of the procedure of future climate and LUCC impact on future runoff. Our climate change versus LUCC impact assessments include four modules. To predict climate scenarios in the future, the DBC method is used to correct climate projections. Future LUCC scenarios LUCC2020–LUCC2050 are simulated by the CA-Markov model. The SWAT distributed hydrological model is used to simulate and project the response of runoff. In the runoff assessment module, both uncertainty analysis, trend and periodicity analysis as well as contribution rate analysis of each driving factor are conducted. For sake of uncertainty representation, a multi-model ensemble involving ten GCMs under RCP4.5 were employed. To eliminate the possible deviation of the hydrological model, future runoff is compared with the simulated runoff in the reference period, which is suggested by numerous studies (Wang et al., 2017; Yin et al., 2018)

3.1 Statistical downscaling of GCM outputs

Since GCM outputs are usually too coarse to represent the climate variability at a basin scale, downscaling methods are needed. In this study, an empirical statistical downscaling approach, i.e. a daily bias correction (DBC) method is employed to reduce the biases of GCMs outputs, which is proposed by Chen et al. (2013). The DBC method is a hybrid method to correct climate projection, which integrates the advantages of the local intensity scaling (LOCI) method (Schmidli et al., 2006) and the daily translation (DT) method (Mpelasoka and Chiew, 2009). The LOCI method is used to correct the frequency of the precipitation. A wet-day threshold at a specific month in the historical period is defined by GCM, to guarantee that the threshold excess value is equal to the number of wet-days observed in the same period. Then the threshold is applied to correct the GCM output frequency in the future corresponding month. The DT method is used to correct the distribution of precipitation and temperature. The calculation equations are as follows (Chen et al., 2013):

$$P_{G,m}^{\mathrm{cor}} = P_{G,m}^{\mathrm{raw}} \times \left(F_{\mathrm{obs}P,m}^{-1}[F_{GP,m}(P_{G,m})]/P_{G,m}\right), \quad (1)$$

$$T_{G,m}^{\mathrm{cor}} = T_{G,m}^{\mathrm{raw}} + \left(F_{\mathrm{obs}T,m}^{-1}[F_{GT,m}(T_{G,m})] - T_{G,m}\right), \quad (2)$$

where $P_{G,m}^{\mathrm{cor}}$ and $P_{G,m}^{\mathrm{raw}}$ ($T_{G,m}^{\mathrm{cor}}$ and $T_{G,m}^{\mathrm{raw}}$) are the daily precipitation (temperature) series of the mth month with and without correction for the future period, respectively; $F_{\mathrm{obs}P,m}^{-1}$ and $F_{GP,m}$ ($F_{\mathrm{obs}T,m}^{-1}$ and $F_{GT,m}$) are the cumulative distribution function of daily precipitation (temperature) measured and GCM-simulated series in the reference period, respectively; $P_{G,m}$ ($T_{G,m}$) is the observed precipitation (temperature) during the reference period.

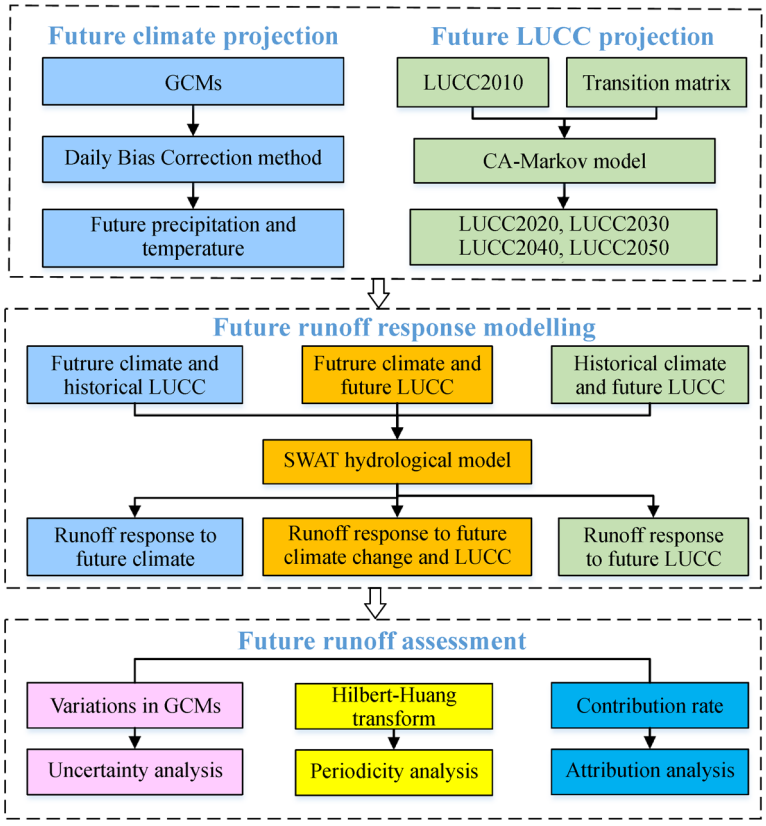

Fig. 2 Flowchart of the procedure of future climate and LUCC impacts on future runoff.

3.2 CA-Markov model

In this study, future LUCC scenarios are simulated based on the CA-Markov model of IDRISI SELVA 17.0 software platform. The CA (Cellular Automata) model characterizes spatial pattern change by fitness maps (Guan et al., 2011; Halmy et al., 2015), which can be defined as Eq. (3):

$$A = (G,U,E,f_x), \tag{3}$$

where A is the results of cellular automata model; G is the cellular grid; U is the cellular neighborhood; E is the initial state set of the cell; f_x is the local space conversion rules of the cell.

The Markov chain procedure controlling temporal variation of different types of land use is represented by a transition matrix, which is defined as Eq. (4):

$$S_{t+1} = P \times S_t, \tag{4}$$

where S_{t+1} and S_t are the system states at $t+1$ and t period, respectively; P is the transition probability matrix in a state.

CA model has a strong ability to simulate the spatial dynamic analysis and evolution of complex space, and has a strong spatial concept. Compared with the CA model, the Markov model has a stronger ability to simulate and predict the change of LUCC quantity, but it cannot predict the change trend of LUCC types in spatial distribution. The CA-Markov model fully combines the spatial dynamic simulation ability of the CA model and the numerical simulation ability of Markov model. It not only improves the prediction accuracy of LUCC type in time, but also realizes the effective simulation of LUCC spatial change (Nouri et al., 2014; Hyandye and Martz, 2017).

To make the future LUCC simulation close to land use strategy and government planning, the specific steps of the CA-Markov model we used are as follows: 1) Markov model is used to calculate the transition matrix of LUCC from historical LUCC maps; 2) The transition matrix is modified according to the planned area of various land use types in the land use master plan (2006–2020) of the basin; 3) In the multi criteria evaluation module, the suitability maps are generated according to the evaluation index; 4) The spatial distribution of LUCC is simulated by the CA model based on the transition matrix and suitability maps. It should be noted that step 2 is the key to ensure that the LUCC simulation conforms to the actual planning.

The Kappa coefficient is usually adopted to assess the consistency between the observed map and the simulated map (Memarian et al., 2012), and is used to evaluate the performance of the CA-Markov model:

$$\text{Kappa} = \frac{P_0 - P_c}{1 - P_c}, \tag{5}$$

where P_0 is the ratio of the correct simulated cells; P_c is the ratio of correct simulation in the random case. If $0.75 < \text{Kappa} \leqslant 1$, then the consistency between the two maps is high and the simulation effective; if $0.4 \leqslant \text{Kappa} \leqslant 0.75$, the consistency between the two maps is at a medium level; and if $\text{Kappa} < 0.4$, the difference between the two maps is large and the similarity is low.

3.3 Hydrological model

The SWAT model is a distributed hydrological model developed by the USDA-ARS, which can simulate and project the changes in hydrological variables on different time scales in large and complex basins (Abbaspour et al., 2007; Gassman et al., 2007; Liang et al., 2018; Li et al., 2019). In the SWAT model, the whole basin is first divided into several sub-basins according to terrain factors and river network distribution. Then, the hydrological response unit (HRU) is further divided based on the land use type, soil type, and slope area threshold of the basin, and the runoff is calculated separately. Finally, the total runoff of the outlet section is obtained through the river confluence routing (Wagner et al., 2013; Zhou et al., 2013; Zhang et al., 2016a). According to the water balance principle, the water quantity calculation of the SWAT model follows the following equation:

$$SW_t = SW_0 + \sum_{t=1}^{n}(R - Q_s - ET - S - QR), \quad (6)$$

where SW_t is the final soil moisture content (mm); SW_0 represents the initial soil moisture content (mm); t is the time step (day) of the model simulation; R, Q_s, and ET are the precipitation (mm), surface runoff (mm), and actual evapotranspiration (mm), respectively; S represents the infiltration and side flow of the bottom layer of the soil profile (mm); QR represents the groundwater flow (mm).

The SUFI-2 algorithm in SWAT-CUP is used to determine the parameters of the SWAT model. The Nash-Sutcliffe coefficient (NSE) and the relative error of water volume (RE) are selected as goodness-of-fit indices to assess the performance of the SWAT model (Pan et al., 2017), as shown in Eqs. (7) and (8):

$$NSE = 1 - \sum_{t=1}^{n}\left(Q_o^t - Q_s^t\right)^2 / \sum_{t=1}^{n}\left(Q_o^t - \overline{Q_o}\right)^2, \quad (7)$$

$$RE = \left[\left(\sum_{t=1}^{n} Q_s^t - \sum_{t=1}^{n} Q_o^t\right) / \sum_{t=1}^{n} Q_o^t\right] \times 100\%, \quad (8)$$

where Q_o^t is the measured value; Q_s^t is the simulated value; $\overline{Q_o}$ is the measured average value; n is the number of measured data.

The meteorological data after statistical downscaling of GCM (Section 2.1) is input into the SWAT model to simulate the runoff of historical and future periods. To analyze the future runoff response to single or combined climate change and LUCC in the next 40 years, based on the baseline scenario (historical climate during 1966–2005 and historical LUCC2010, and runoff under baseline scenario is expressed as $Q_{b.}$), the following scenarios of future climate and LUCC combination are set up: 1) climate change scenario (combined climate change during 2021–2060 and historical LUCC2010), the runoff is expressed as $Q_{HL4.5}$; 2) LUCC scenario (combined historical climate during 1966–2005 and FL (future LUCC2020– LUCC2050)), the runoff is expressed as Q_{FL} ; 3) Combined climate change and LUCC scenario (combined future climate during 2021–2060 and FL), the runoff is expressed as $Q_{FL4.5.}$ It should be noted that: the meteorological data of 2021–2030, 2031–2040, 2041–2050, and 2051–2060 correspond to LUCC2020, LUCC2030, LUCC2040, and LUCC2050, respectively.

3.4 Runoff assessment methods

3.4.1 Hilbert-Huang Transform

Hilbert Huang Transform (HHT) is a time-frequency analysis method for nonlinear and non-stationary data proposed by Huang et al. (1998). HHT method breaks away from the limitation of a traditional Fourier transform. Compared with wavelet transform (WT), the HHT method usually has three advantages: 1) The intrinsic mode function (IMF) of HHT obtained with empirical mode decomposition (EMD) can reflect the intrinsic physical characteristics of original data and it has no need of using base functions, while selecting a mother wavelet is a difficulty problem in WT (Huang et al., 1999); 2) Hilbert energy spectrum in HHT can clearly express the energy distribution with time and frequency in detail, and most energy is concentrated in a definitive range of time and frequency, but that of wavelet spectrum lines in WT are distributed in a wider frequency range (Shen et al., 2003); 3) The resolving power of time and frequency is restricted from Heisenberg principle in WT, while in HHT time resolving power is precise and steady, and frequency resolving is adaptive according to signal intrinsic characteristics (Senroy et al., 2007).

The HHT method mainly includes two parts (Huang et al., 1998): 1) The basic idea is to obtain several intrinsic mode functions (IMFs) from time-series through empirical mode decomposition (EMD); 2) Hilbert transform is applied to each IMF, then the instantaneous frequencies and the period of each IMF component in time series are obtained. Since the decomposition is based on the time scale characteristics of the data itself and has no prior basis, the HHT method is applicable to nonlinear and non-stationary processes. After obtaining the IMFs, the steps of

Hilbert transform for each IMF are shown in Eqs. (9)–(13) (Huang et al., 1998).

For an arbitrary time series $X_i(t)$, its Hilbert Transform $Y(t)$ can be shown as

$$Y(t) = \frac{1}{\pi} P \int_{-\infty}^{\infty} \frac{X_i(t')}{t-t'} \mathrm{d}t', \quad (9)$$

where $X_i(t)$ is a given time series (represents runoff series in this study); $Y(t)$ is the Hilbert Transform of $X_i(t)$; P indicates the Cauchy principal value. With this definition, $X_i(t)$ and $Y(t)$ form a complex conjugate pair, so an analytic signal $Z_i(t)$ can be shown as

$$Z_i(t) = X_i(t) + iY(t) = a_i(t)e^{i\theta_i(t)}, \quad (10)$$

where $a_i(t)$ and $\theta_i(t)$ are the instantaneous amplitude and frequency, which are defined as

$$a_i(t) = [X_i{}^2(t) + Y^2(t)]^{1/2}, \quad (11)$$

$$\theta_i(t) = \arctan\Big(Y(t)/X_i(t)\Big). \quad (12)$$

The instantaneous frequency $W_i(t)$ is defined as

$$W_i(t) = \mathrm{d}\theta_i(t)/\mathrm{d}t. \quad (13)$$

3.4.2 Contribution rate of the driving factors

The contribution rate is used to separate the impacts of future climate change and LUCC on runoff process (Zhang et al., 2016b). When compared $Q_{HL4.5}$ (the runoff under combined future climate and historical LUCC) with Q_b (the runoff under baseline scenario), we can find that only climate factor is different, so the difference between them can be regarded as the impact of RCP4.5 on runoff. The difference between $Q_{FL4.5}$ (the runoff under combined future climate and future LUCC) and Q_{FL} (the runoff historical climate under future LUCC) can also be considered as the impact of the RCP4.5. Hence, the mean value of the two is used to calculate the impact of RCP4.5 (Eq. (14)). Similarly, the difference between Q_{FL} and Q_b or $Q_{FL4.5}$ and $Q_{HL4.5}$ can be considered as the effect of FL on runoff, which can be calculated according to Eq. (15):

$$\Delta Q_{\mathrm{RCP4.5}} = [(Q_{HL4.5} - Q_b) + (Q_{FL4.5} - Q_{FL})]/2, \quad (14)$$

$$\Delta Q_{FL} = [(Q_{FL} - Q_b) + (Q_{FL4.5} - Q_{HL4.5})]/2. \quad (15)$$

Then, the contribution rate of RCP4.5 ($\theta_{\mathrm{RCP4.5}}$) and FL (θ_{FL}) on runoff change can be calculated as Eq. (16) and Eq. (17):

$$\theta_{\mathrm{RCP4.5}} = \Delta Q_{\mathrm{RCP4.5}}/(\Delta Q_{\mathrm{RCP4.5}} + \Delta Q_{FL}), \quad (16)$$

$$\theta_{FL} = \Delta Q_{FL}/(\Delta Q_{\mathrm{RCP4.5}} + \Delta Q_{FL}). \quad (17)$$

4 Results

4.1 Model calibration and performance evaluation

4.1.1 Performance of DBC method

The period from 1966 to 2005 is divided into the calibration period (1966–1990) and the validation period (1991–2005). The performance of the DBC method is verified on the basis of six observation statistics. Here, we take the validation results of the RCP4.5 scenario as an example. Figs. 3(a)–3(f) show the deviation of precipitation and temperature of GCMs on daily time scales at the validation period. The values of the grids indicate the relative error and absolute error of the daily precipitation and temperature simulation series relative to the measured series. The X-axis represents ten selected GCMs and the Y-axis represents 6 indicators: 1) mean; 2) standard deviation; 3) 50th percentile; 4) 75th percentile; 5) 90th percentile and 6) 95th percentile. It can be seen from Fig. 3 that the average value of the simulated precipitation series before correction is higher, the standard deviation is lower, the 50th, 75th, and 90th percentiles are higher, and the 95th percentile is lower compared with the measured series. The results show that the GCMs outputs overestimate average precipitation and underestimate extreme precipitation. After correction, the relative errors of the evaluation indicators of the precipitation series were reduced to within 5%, and the absolute errors of the indicators of the temperature series were within 1.5°C, indicating that the DBC method has a good correction effect on the daily precipitation, minimum and maximum temperatures in the Han River basin.

Figures 3(g)–3(h) show the precipitation occurrence probability biases of raw and corrected GCMs. The value of the grid in the figure represents the deviation of the wet day percentage of the GCM simulated precipitation series relative to the measured series. Before downscaling, the monthly wet day percentages of the simulated rainfall series at ten GCMs are significantly higher (+55%), which overestimates the frequency of precipitation. But after correction, the percentage of wet days at each month of ten GCMs are all very close to the measured series, and the deviation of all stations is basically within ±15%. The above results show the performance of the DBC method is good, and the rationality of its application in future climate change scenarios study.

4.1.2 Performance of the CA-Markov Model

To evaluate the performance of the CA-Markov model, the

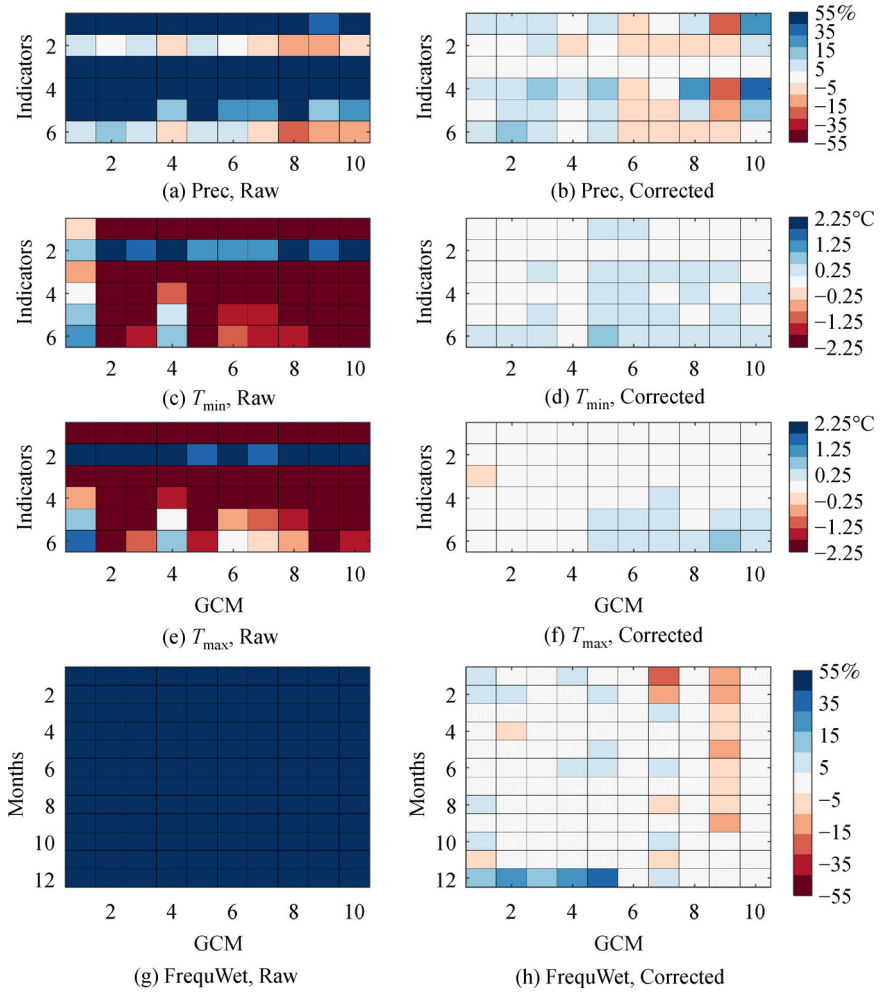

Fig. 3 Evaluation of precipitation and temperature simulation results of raw and corrected GCM outputs in the Han River basin.

observed LUCC1990 and LUCC2000 are first input into the model for superposition analysis to obtain the transition probability matrix between LUCC1990 and LUCC2000 in the Han River basin. Secondly, considering the actual topographic and geomorphic conditions of the basin and the development of urban areas and other factors, the elevation, slope, distance to cities and villages, and distance to traffic lines is picked to generate transition suitability maps of LUCC. Eventually, based on observed LUCC2000 and the transition probability matrix and suitability maps, the LUCC2010 of the Han River basin is simulated by the CA-Markov model (as shown in Fig. 4(b)). Using the crosstab module in the CA-Markov model, the observed LUCC2010 and the simulated LUCC2010 in the Han River basin are compared, and the Kappa coefficient is calculated as 0.9 (greater than 0.75), indicating that the CA-Markov model has a good performance and can be used to project the future LUCC scenario in the Han River basin.

Each LUCC model has its own capabilities and limitations. A single model is not capable of capturing all of key processes in a land use change projection (Luo et al., 2010). In this study, there are three uncertainty sources of the LUCC prediction process (Pontius et al., 2010). 1) The data. Typical natural and socioeconomic indicators are needed to compute transition potential maps of land use scenarios. If data are scarce and data selection is not free, the accuracy of simulation results will be affected. 2) The model. The CA-Markov model is based on a set of rules that take into account changes between land-use classes, the suitability of cells, and the land use of neighborhood cells (Halmy et al., 2015). In this regard, it is a simple and straightforward approach and can be applicable for spatial land-cover reconstructions of land-use. However, it does not consider changes to driving factors, does not sufficiently differentiate between suitable locations and does not allow differentiation of neighborhood filter rules. These characteristics may complicate its application and lower the quality of reconstructions (Poska et al., 2008). And 3) future land change processes. As the future land use is related to the policies made by the government and changes with time, it has uncertainty in

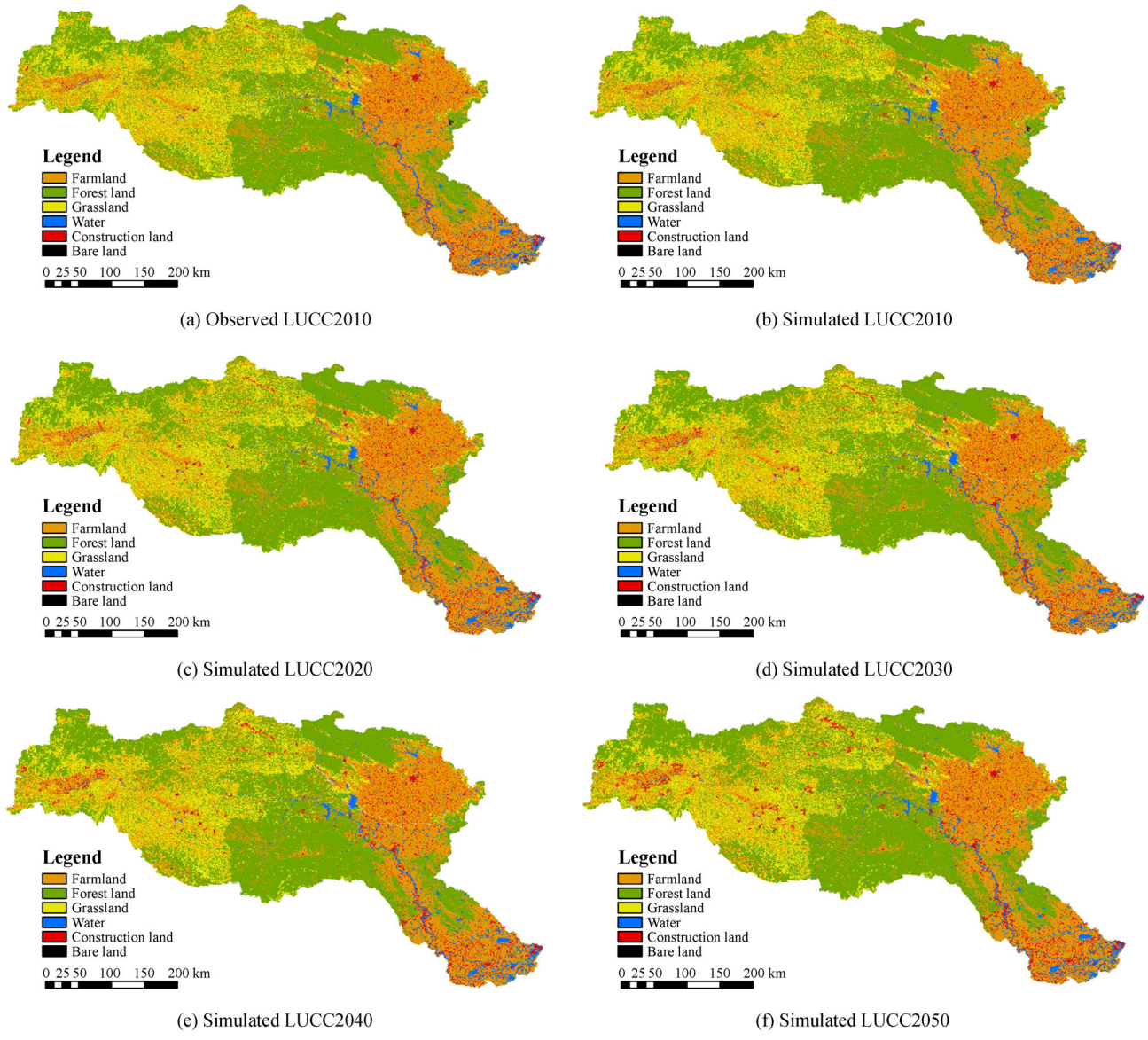

Fig. 4 Measured and simulated LUCC of Han River basin.

future land change processes, so the transfer matrix needs to be modified artificially.

In this study, we selected typical natural and socio-economic indicators (including slope, elevation, distribution of road/railway/city and town, river network) to compute transition potential maps of land use scenarios. In addition, the transfer matrix is modified according to land use strategy and government planning. The resulting Kappa coefficient shows that the prediction results of LUCC2010 follows the measured map LUCC2010, implying that there is certain feasibility in respect of the utilization of the CA-Markov model on the prediction of land use changes. However, more deterministic socio-economic parameters on land use changes should be considered such as population growth, for the purpose of enhancing accuracy of the prediction.

4.1.3 Performance of the SWAT Model

Based on the measured runoff data from 1980 to 2000, 1980–1993 is selected as the calibration period and 1994–2000 is selected as the validation period. The results of sensitivity analysis using SWAT-CUP and the calibration results of sensitivity parameters of the SWAT model are shown in Table 2. ALPHA_BF, CH_K2, CH_N2, CN2, GW_DELAY, GW_REVAP, GWQMN, ESCO, SFTMP, SOL_BD, SOL_AWC, and SOL_K are the first 12 sensitivity parameters for the simulated runoff. Table 2 shows that parameters representing soil property and base flow are much more sensitive. The simulation performances of the four hydrological stations at calibration and validation periods are shown in Fig. 5, on which shows that the *NSE* value of each hydrological station is greater than

0.8, and the values of *RE* are all within 15%. Figure 6 shows the observed and simulated monthly runoff hydrographs at four hydrological stations. Overall, the absolute average values of *NSE* and *RE* at the calibration and validation periods are 0.89, 4.1%, and 0.76, 7.9%, respectively, indicating that the SWAT model performs well in the Han River basin.

4.2 Projection of future climate change and LUCC scenarios

4.2.1 Future climate scenarios

Applying the DBC method to the future output sequences of ten GCMs, the future precipitation and temperature changes in the Han River basin under the two representative concentration paths of RCP4.5 and RCP8.5 are estimated.

Figure 7 shows the relative change of mean annual precipitation and the absolute change of mean daily temperature in future years. In the figure, each boxplot was constructed using 10 values derived from 10 GCMs. The 40 boxplots in one subgraph represent 40 future periods. Under RCP4.5, the ensemble median of annual precipitation increased from 2.99% for 2021–2040 to 3.16% for 2041–2060. Under RCP8.5, the ensemble median of annual precipitation increased from 1.80% for 2021–2040 to 6.25% for 2041–2060. In 2021–2040, RCP4.5 predicted a more rapid increase in precipitation than RCP8.5. However, in 2041–2060, the trend is opposite. In addition, all GCMs predicted increase in daily temperature for both RCP4.5 and RCP8.5 representative concentration paths and all future periods. The maximum and minimum temperature all show a larger and more rapid increase in RCP8.5 than those in RCP4.5. For example, the maximum temperature was predicted to be a

Table 2 Parameters sensitivity analysis and calibration results of the SWAT model

Parameter	Description	Sensitivity analysis		Calibration
		t-statistics	*p*-value	Fittedvalue
ALPHA_BF	The extinction coefficient of base flow	–2.34	0.02	0.5
CH_K2	Hydraulic conductivity coefficient of river	0.93	0.36	70.06
CH_N2	Manning coefficient of river	0.71	0.48	0.06
CN2	Runoff curve number Ⅱ for moisture condition	1.69	0.09	–0.18
GW_DELAY	Delayed recharge time of aquifer (d)	–1.95	0.05	184.35
GW_REVAP	Evaporation coefficient of groundwater	–0.93	0.36	0.1
GWQMN	Depth of water in the shallow aquifer (mm)	–1.03	0.31	0.46
ESCO	Soil evaporation compensation coefficient	–1.48	0.14	1.06
SFTMP	Base temperature of snowmelt (°C)	2.07	0.04	–3.39
SOL_BD	Wet bulk density (mg/m^3)	3.68	0	0.26
SOL_AWC	Soil available water content (mm)	1.49	0.14	0.38
SOL_K	Saturated permeability coefficient of the first soil layer (mm/h)	3.39	0	–0.43

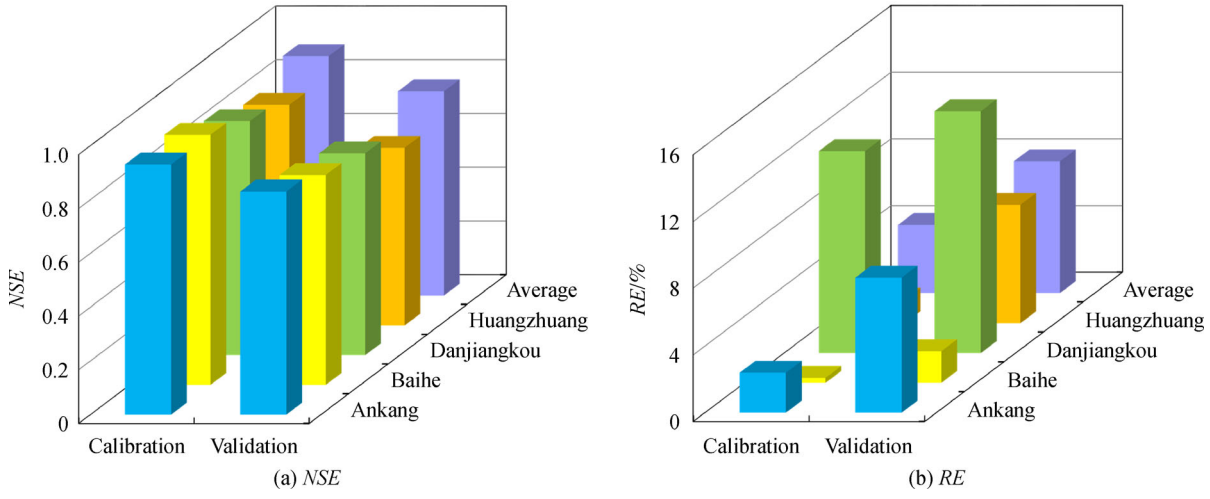

Fig. 5 Calibration and validation results of the SWAT model.

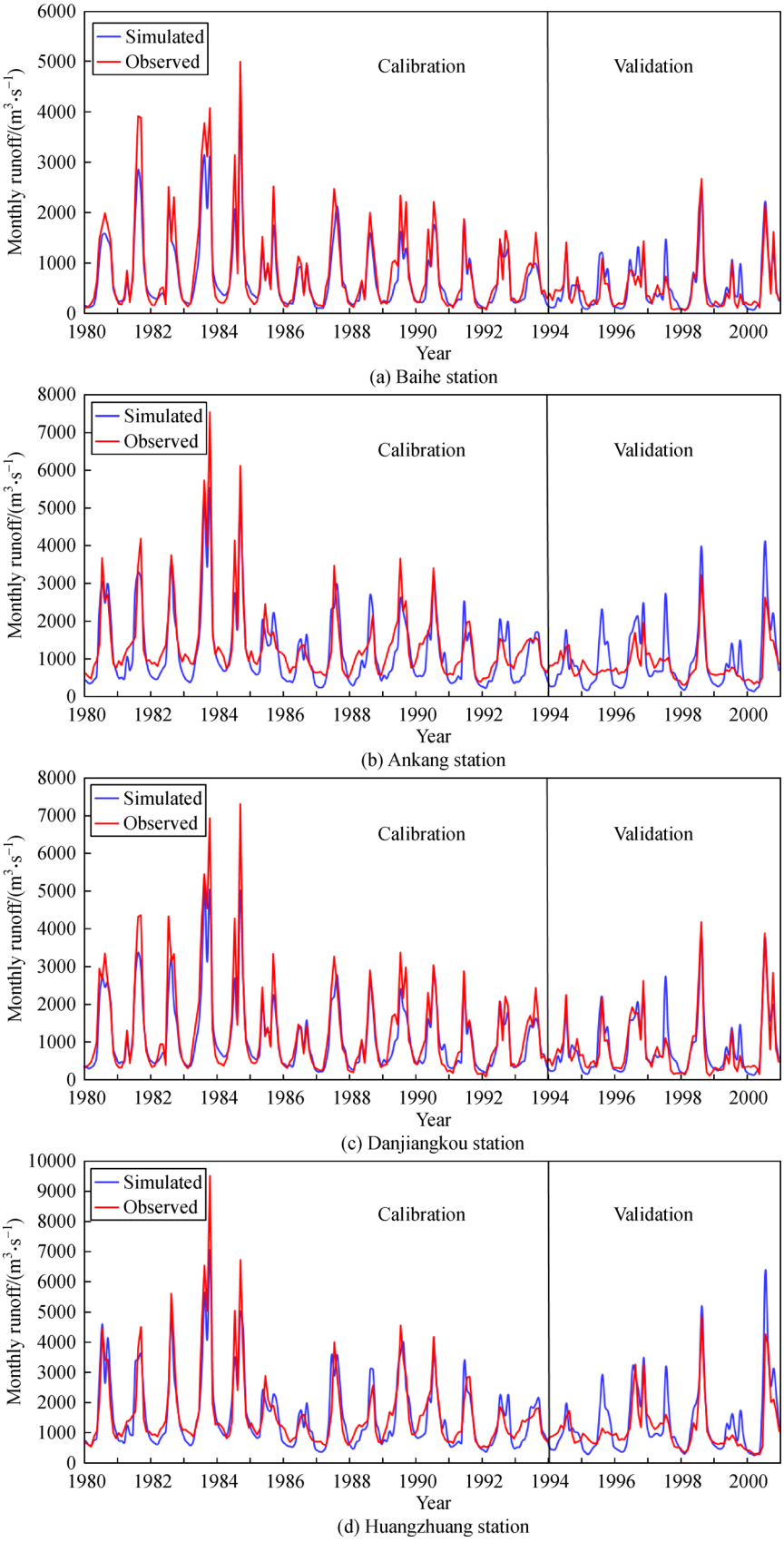

Fig. 6 Observed and simulated monthly runoff hydrographs at four hydrological stations.

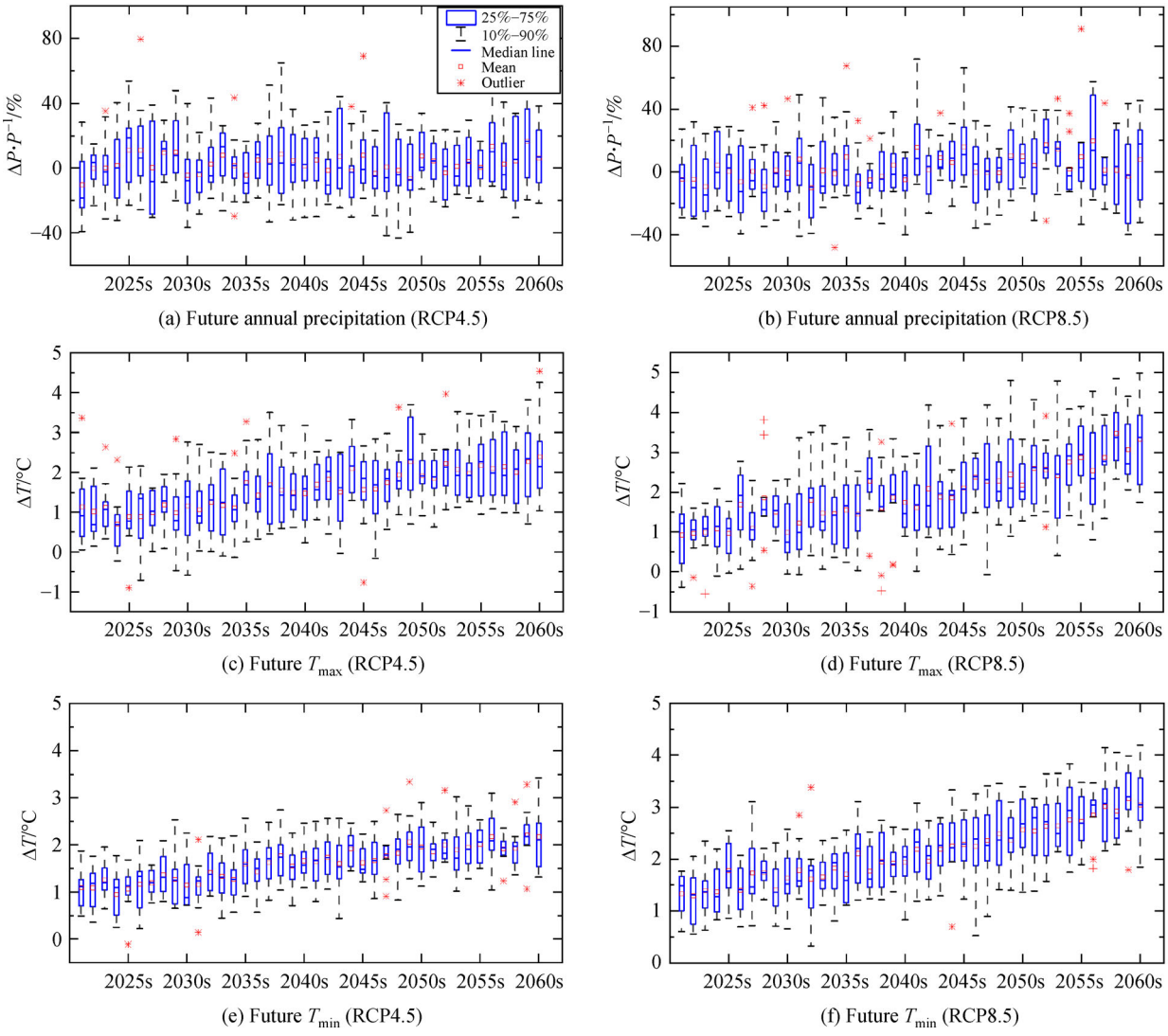

Fig. 7 Future climate change projected by the ten bias-corrected GCMs under RCP4.5.

1.23°C increase in RCP4.5 for 2021–2040 and a 2.01°C increase for 2041–2060 in terms of the median of the ten GCMs, while RCP8.5 predicted a 1.44°C increase for 2021–2040 and a 2.57°C increase for 2041–2060. The minimum temperature for 2021–2040 was predicted to be a 1.23°C and 1.34°C increase in terms of the median of the ten GCMs in RCP4.5 and RCP8.5, respectively. And for 2041–2060 it was predicted to be a 1.66°C and 2.56°C increase in RCP4.5 and RCP8.5, respectively.

The annual average changes of precipitation and temperature from the ten GCMs are statistically listed in Table 3. The annual precipitation and daily maximum and minimum temperatures in the Han River basin in the future period will all increase compared with the base period. Under RCP4.5 and RCP8.5, they will increase by 42.59 mm (+ 5.07%), 1.55°C, and 1.46°C, and 50.89 mm (+ 6.06%), 2.10°C, and 1.96°C, respectively, for 2021–2060.

4.2.2 Future LUCC scenarios

Future maps of LUCC2020, LUCC2030, LUCC2040, and LUCC2050 in the Han River basin are projected by the CA-Markov model on the basis of LUCC2010, the suitability maps, and the transition matrix between LUCC2000 and LUCC2010. LUCC2020 and LUCC-2050 are shown in Figs. 4(c) and 4(f), respectively. Comparing Figs. 4(c) and 4(b), the construction land represented by red and the forest land represented by green will increase significantly. Comparing Figs. 4(d) and 4(c), construction land and forest land in 2030 will have further increased. The reason is that the CA-Markov model maintained the land use change trend between LUCC2010 and LUCC2020 to simulate LUCC2030 to LUCC2050. For ease analysis of variation of each LUCC type, the percentages of each LUCC type area in each year are listed in Table 4. It can be seen that: 1) from 2010 to 2050, the

Table 3 The annual average variation of GCMs ensemble of precipitation and temperature in the future periods.

The whole basin	Base period (1966—2005)	Future (2021—2060)			
		RCP4.5		RCP8.5	
	Average	Average	Change	Average	Change
Precipitation/mm	839.91	882.50	+42.59	890.80	+50.89
T_{max}/°C	20.29	21.84	+1.55	22.39	+2.10
T_{min}/°C	10.52	11.98	+1.46	12.48	+1.96

Table 4 Percentages of future LUCC type area in the Han River basin (%).

Land use type	Historical	Future			
	2010	2020	2030	2040	2050
Farmland	35.2	34.5	34.2	33.9	33.7
Forest land	40.0	41.0	41.4	42.0	42.8
Grassland	19.2	18.6	18.3	17.7	16.7
Water bodies	2.8	2.8	2.8	2.8	2.8
Construction land	2.7	3.0	3.2	3.5	3.9
Bare land	0.1	0.1	0.1	0.1	0.1

forest land and construction land in the Han River basin will increase by 2.8% and 1.2%, respectively; 2) the farmland and grassland area will decrease by 1.5% and 2.5%, respectively; 3) the water bodies and bare land will be unchanged. In 2050, the largest proportion of land use types is still forest land, followed by farmland, grassland, construction land, and water bodies.

4.3 Runoff response to future climate change and LUCC

4.3.1 Runoff response to future climate change

To analyze runoff response to climate change at the spatial scale, the future runoff variation of four hydrological stations in the mainstream under RCP4.5 and RCP8.5 are shown in Fig. 8. Compared with the mean annual runoff of BH_b (baseline of Baihe), AK_b (baseline of Ankang), DJK_b (baseline of Danjiangkou) and HZ_b (baseline of Huangzhuang) in 1966–2005, the mean annual runoff of four stations in 2021–2060 under RCP4.5 and RCP8.5 will all increase. And the increase of runoff in RCP8.5 is less than that in RCP4.5. In all 10 GCMs, the models of BCC-CSM1.1, BNU-ESM, CSIRO-Mk3, GFDL-ESM2G, and NorESM1-M all show an increasing trend while the models of CanESM2, CCSM4, CNRM-CM5, MPI-ESM-LR, MRI-CGCM3 all show a decreasing trend in future runoff. The reason is that the rainfall of the former five models are more than that in the historical period, resulting in increase of runoff. And the latter five models show pronounced warming with higher temperature, thus leading to more evaporation and less runoff. The results indicate that the impact of precipitation variation on runoff is direct, and the relationship between them is positive.

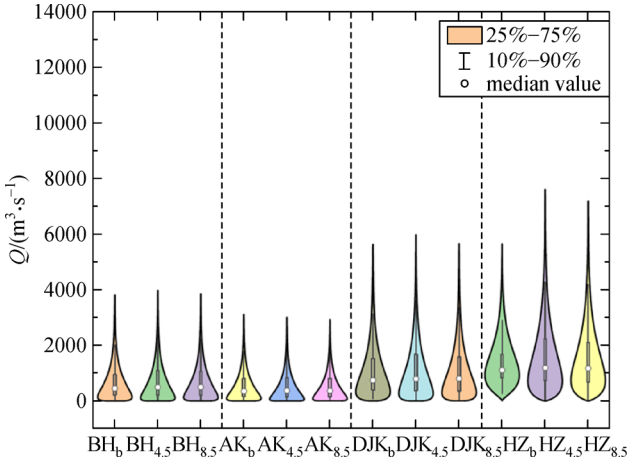

Fig. 8 Comparison of simulated runoff of different stations over Han River basin under the base period and future climate change.

While the impact of temperature variation on runoff is indirect, and the correlation between them is negative. Therefore, the runoff of the former five models is higher while the runoff of the latter five models is lower than that of baseline. However, the results of GCM ensemble mean value show that the runoff is still rising compared with the baseline in whichever hydrological station.

4.3.2 Runoff response to future LUCC

Under the FL scenario, the runoff change at the four stations of Han River basin is shown in Table 5: the multi-year average runoff under FL scenario will change +0.69%, +0.55%, +0.44%, +0.12% compared with the

simulated runoff under the base scenario. Moreover, runoff increases in flood season (May to October) and decreases in the non-flood season (November to April). This phenomenon will aggravate the pressure of flood control and increase the contradiction between water supply and demand in non-flood season, which is not conducive to the future water resources management of Han River basin. In several types of land use, grassland and construction land have high runoff rate, which can effectively increase runoff. Forest land has the effect of water storage and rainfall interception, and thus can effectively save water and reduce runoff. Therefore, with the significant increase of construction land area, runoff in the FL scenario presents an increasing trend. From the perspective of water resources, if decision-makers of the planning department prefer to reduce the flood control pressure in the basin, they should control the continuous increase of construction land area in the future, and change the land converted from farmland to forest land; if the decision-maker focuses on solving the contradiction between water supply and water demand, they might increase the area of future construction land according to the current development trend, and the land converted from farmland should be changed into grassland.

4.3.3 Runoff response to synthetic future climate change and LUCC

Figures 9 and 10 show the runoff variation of the four mainstream hydrological stations under the combined future climate change and LUCC at the annual and monthly scales under RCP4.5 and RCP8.5, respectively. The Figs. 9(a), 9(c), 9(e), 9(g), and Figs.10(a), 10(c), 10(e), 10(g) show the runoff of 10 GCM varied with time 2021–2060. It can be seen that: 1) for RCP4.5, the runoff will be maximized in the year 2025 and minimized in the year 2034 for all stations; for RCP8.5, the runoff for all stations will be maximized in the year 2055 while the minimum runoff appears in different years; 2) runoff under RCP4.5 is significantly higher than that of RCP8.5, and the reason is that there is little difference in rainfall between the two scenarios, while the temperature under RCP8.5 is significantly higher than that of RCP4.5, which leads to an increase in evaporation under RCP8.5; 3) The values between the upper and lower runoff box boundaries are very different, and it presents a fluctuating trend with the sliding of time. The results demonstrate that the simulated runoff under 10 GCMs shows great uncertainty.

The Figs. 9(b), 9(d), 9(f), 9(h) of and Figs. 10(b), 10(d), 10(f), 10(h) show the distribution of monthly runoff of the four stations in both 1966–2005 and 2021–2060. For the ten GCMs, runoff simulated by G1 is the largest while G3 shows the smallest in future runoff simulation at all the four stations. This result is due to the maximum precipitation in G1 while the minimal precipitation in G3 among the 10 GCMs. Among the annual changes, the runoff fluctuation in July and August at all the four stations is the most severe while the runoff variation is more consistent for the 10 GCMs in other months. Moreover, the monthly runoff can be divided into two periods. For Huangzhuang station, the monthly runoff is expected to decline from January to April, leading to a more serious drought in the non-flood season. In contrast, the monthly runoff from May to October is higher than that in baseline, indicating that the flood risk at the station will be higher. It is obvious that Huangzhuang station has a dividing line between flood season and non-flood season under combined future climate change and LUCC. As for Baihe and Ankang stations, almost all GCMs show a downward trend compared with the historical period. For Danjiangkou station, the performance of all GCM in non-flood season is almost the same, but it is very different in flood season. Overall, the results indicate that climate change and LUCC cannot only affect the amount of runoff but also affect the confluence time in the basin.

5 Discussion

5.1 Uncertainty range of future runoff projection

Although uncertainty may be sourced from various procedures in climate change and LUCC impact assessments, the selection of GCM is the biggest one in all

Table 5 Changes of the projected runoff under LUCC in Han River basin (m^3/s)

Period	Baihe			Ankang		
	Q_b	Q_{FL}	variation	Q_b	Q_{FL}	variation
Annual	721	726	0.69%	542	545	0.55%
Flood season	1187	1201	1.17%	898	910	1.29%
Non-flood season	255	252	–1.28%	187	182	–2.60%
Period	Danjiangkou			Huangzhuang		
	Q_b	Q_{FL}	variation	Q_b	Q_{FL}	variation
Annual	1127	1132	0.44%	1607	1609	0.12%
Flood season	1815	1832	0.93%	2451	2486	1.41%
Non-flood season	440	433	–1.55%	764	755	–1.22%

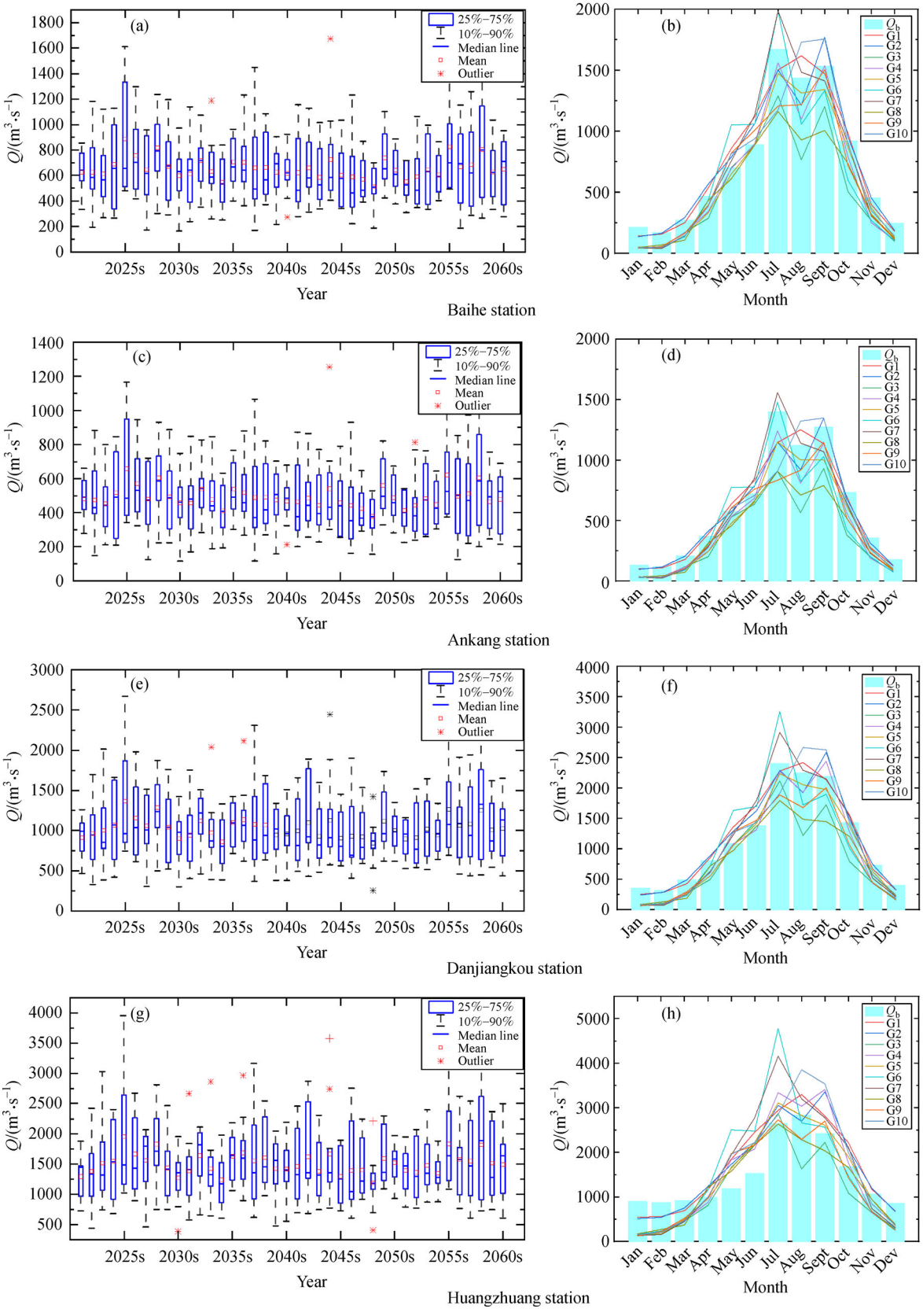

Fig. 9 Annual and monthly runoff over Han River basin in 2021–2060 under climate change (RCP4.5) and LUCC.

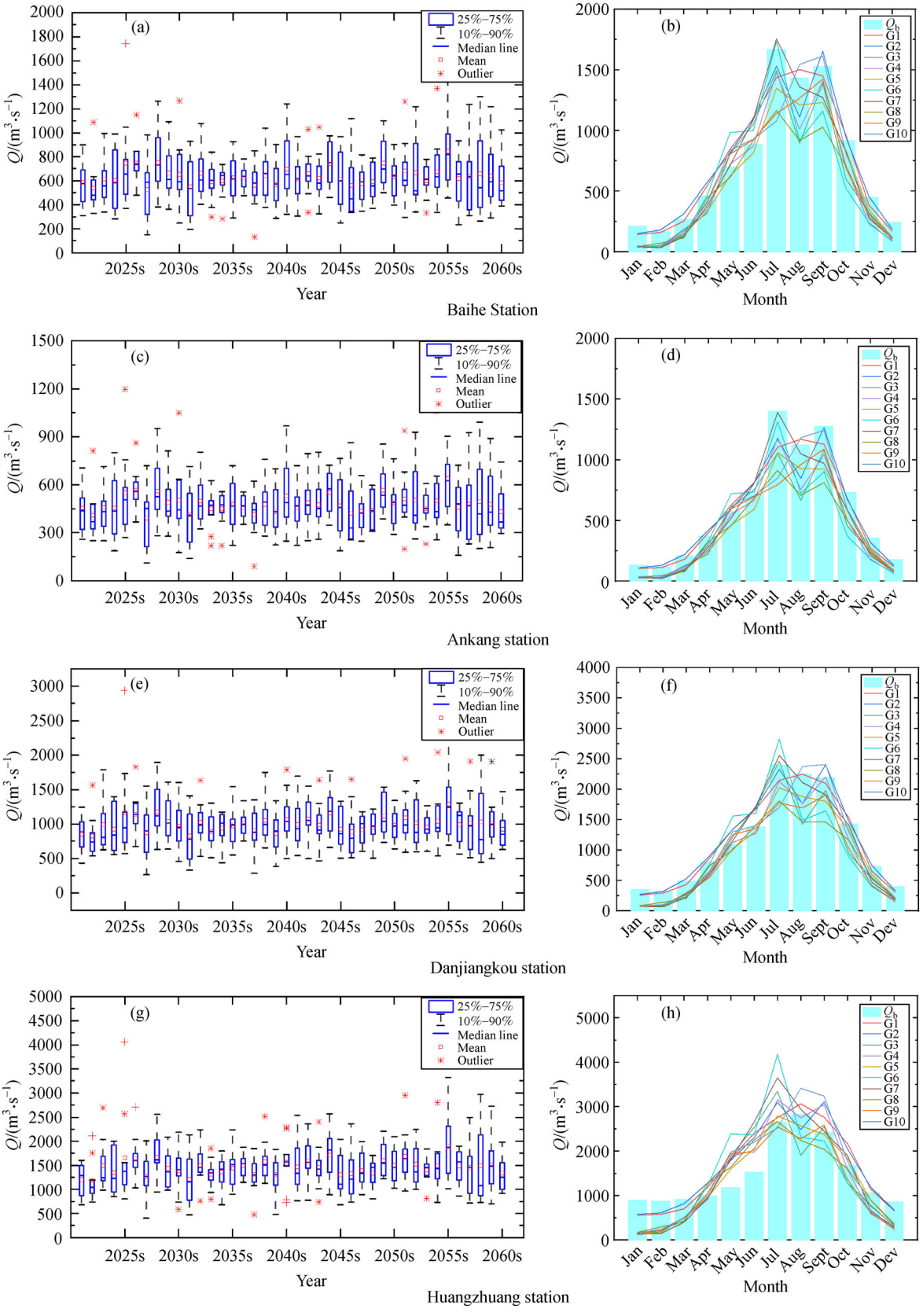

Fig. 10 Annual and monthly runoff over Han River basin in 2021–2060 under climate change (RCP8.5) and LUCC.

sources. In this study, a multi-model ensemble of ten GCMs is used to explore the underlying uncertainty. The interval of precipitation, temperature, and runoff under different GCMs is used to represent the uncertainty. The uncertainty range of future daily precipitation and temperature over Han River basin is shown in Fig. 11. For RCP4.5, we can see that the relative change of daily precipitation in the future (2021–2060) is from −43.32% to +79.47% compared with the historical period, while the uncertainty range of the GCM ensemble median of daily precipitation is approximately [–10.28%, +16.62%]. The ranges of daily T_{max} and T_{min} change are [–0.9°C, +4.54°C] and [–0.12°C, +3.43°C], respectively. For RCP8.5, The ranges of daily precipitation, T_{max} and T_{min} are [–48.42%, +90.95%], [–0.55°C, +4.98°C] and [+0.03°C, +4.20°C], respectively. The results show that there are significant differences among the simulation results of different GCMs, which proves that GCM is a big factor leading to the uncertainty. Figure 12 shows the uncertainty range of future runoff projection of four hydrological stations over the mainstream of the Han River basin. The relative changes at Baihe, Ankang, Danjiangkou, and Huangzhuang station are mainly in [–50%, +50%] for both RCP4.5 and RCP8.5. As for the GCM ensemble median for runoff, the relative change of Baihe, Ankang, Danjiangkou, and Huangzhuang station all fluctuated up and down about zero, which means that the GCM ensemble median results can reduce the error and uncertainty of runoff projection. Therefore, when evaluating the impact of climate change on future hydrology and water resources in a basin, it is likely to use results of multiple GCMs to avoid biased conclusions.

From the comparison of uncertainty interval between precipitation and runoff, the uncertainty range of runoff is much larger than that of precipitation. The results show that the uncertainty of runoff comes not only from GCM but also from the downscaling method and hydrological model used, which aggravate the uncertainty in projecting runoff.

To improve the accuracy of runoff simulation, it is necessary to consider the influence of reservoir regulation on runoff simulation. However, due to the complexity of reservoir operation, it is very difficult for runoff simulation in large basin. Only a small number of studies considered reservoir regulation in runoff simulation by adding reservoir variables into the hydrological model, and found that the simulation results are similar with or without considering the reservoir regulation when the storage capacity is small. In this study, the impact of reservoir was ignored due to paucity of data, but it will be a focus in our future research.

5.2 Characteristics analysis of future runoff

Figure 13 presents the EMD decomposition results of future runoff series of four hydrological stations (Baihe,

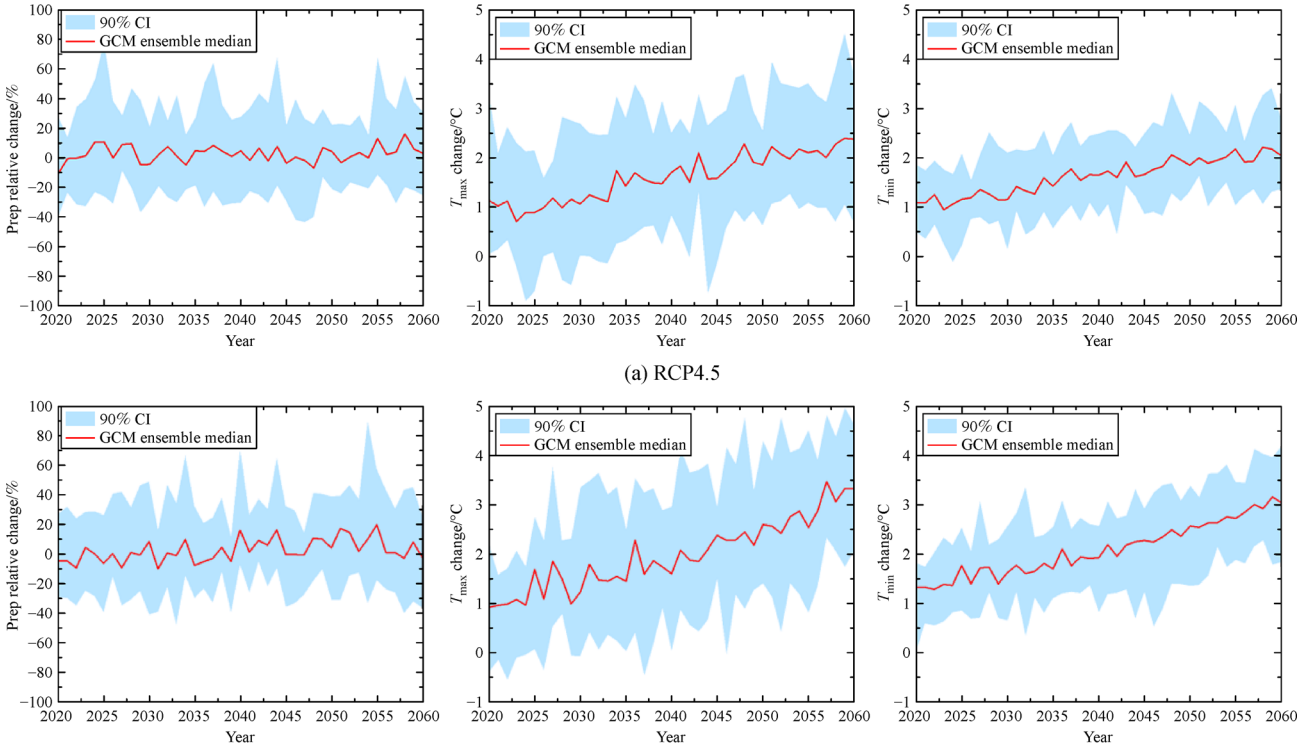

Fig. 11 Uncertainty range of future daily precipitation and temperature over Han River basin.

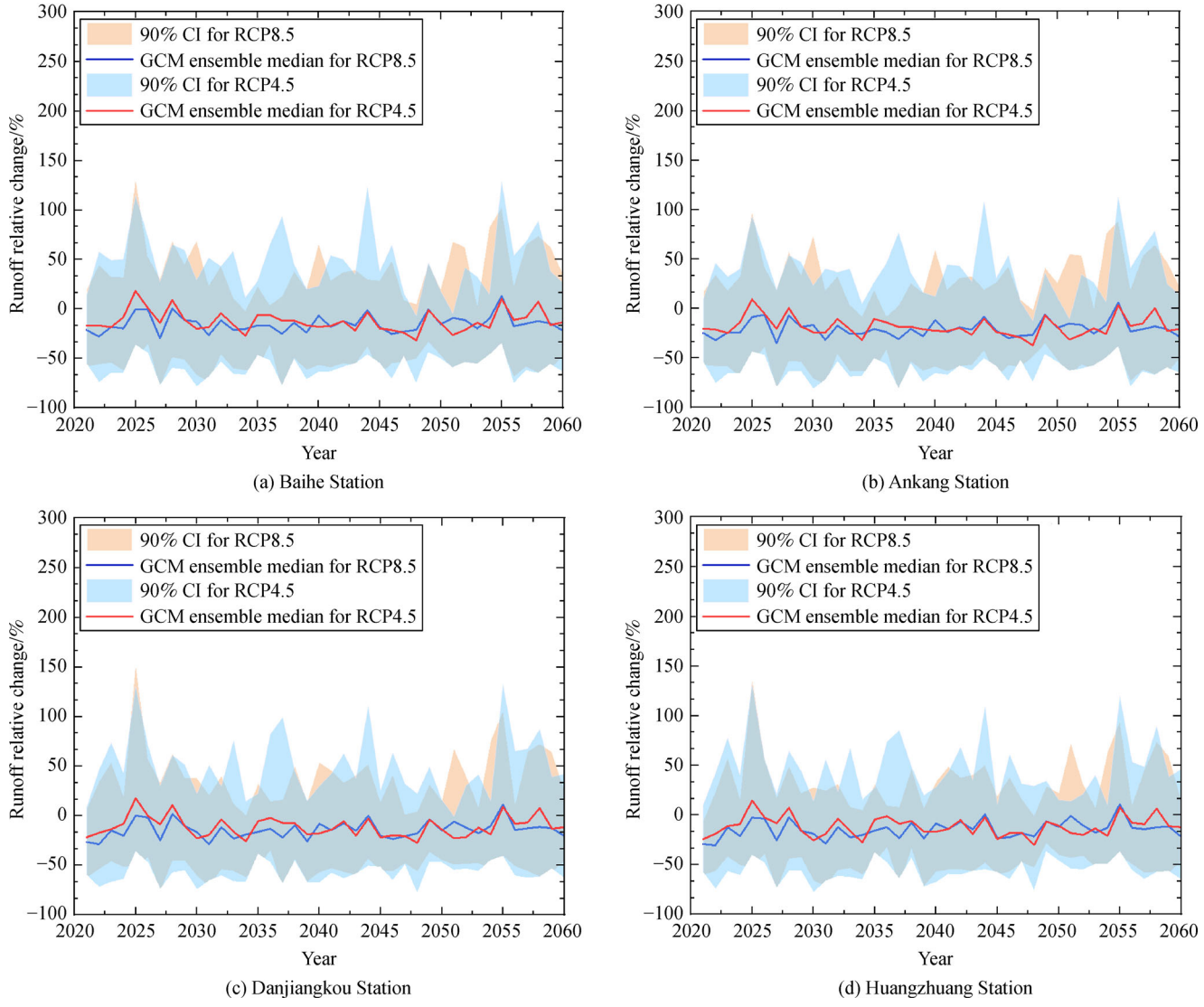

Fig. 12 Uncertainty range of future runoff projection of four hydrological stations over Han River basin.

Ankang, Danjiangkou, and Huangzhuang) from 2021 to 2060. For Baihe station, seven IMFs and a monotonic decreasing trend term have been obtained from the monthly runoff under RCP4.5, while six IMFs and a decreasing then increasing trend term have been obtained under RCP8.5. For Ankang station, six IMFs (under RCP4.5) and five IMFs (under RCP8.5) have been identified in the monthly runoff, future runoff under these two scenarios both show a decreasing then increasing trend term. Furthermore, the monthly runoff of Danjiangkou station under RCP4.5 has been separated into six IMFs and a two-steps tendency through the EMD method. The monthly runoff of Huangzhuang station under RCP8.5 is decomposed into seven IMFs with a projected rising trend.

To derive the potential periodicity of the monthly runoff, the process of the Hilbert transform is used for the IMF components derived by the EMD method. The results show that significant periodicity is detected by Hilbert Transform for all the mean flow at the $P = 0.05$ significance level (Fig. 13). The potential periodicity of four stations is presented in Table 6. For RCP4.5, the IMF components of monthly runoff series at all four stations have been identified with the seasonal (around 3 months), half-year (around 6 months), annual (11–16 months), two-year (24–30 months), five-year (60–61 months), and ten-year (118–122 months) periods. For RCP8.5, the IMF components of monthly runoff series at both four stations have been identified with the seasonal (around 3 months), half-year (around 6 months), annual (11–12 months), two-year (19–29 months), four-year (46–48 months), and ten-year (103–116 months) periods. Since monthly runoff is used instead of the annual runoff obtained by a moving window, this small periodicity will not be filtered out and a significant periodicity is observed. It should be mentioned that since the future runoff simulated in the SWAT model takes a month as the time step, the annual runoff is calculated

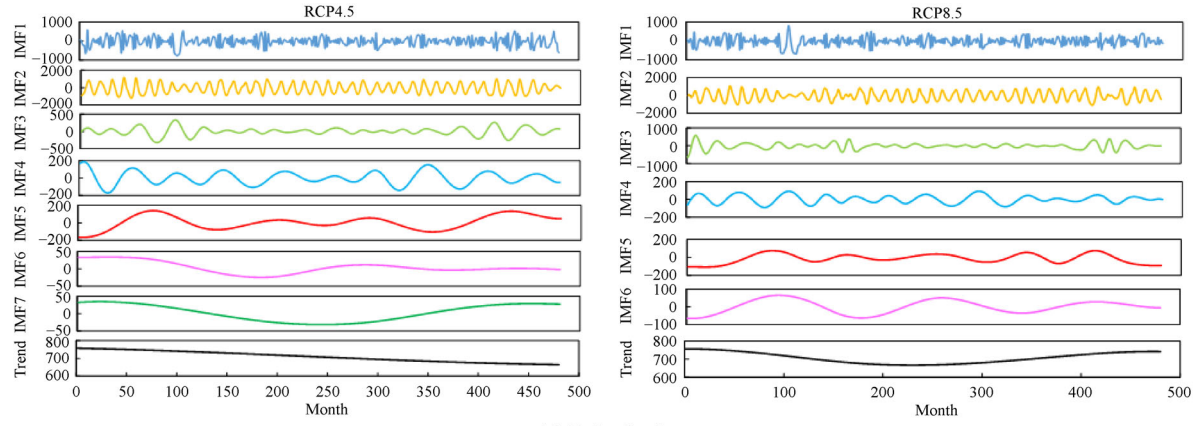

(a) Baihe Station

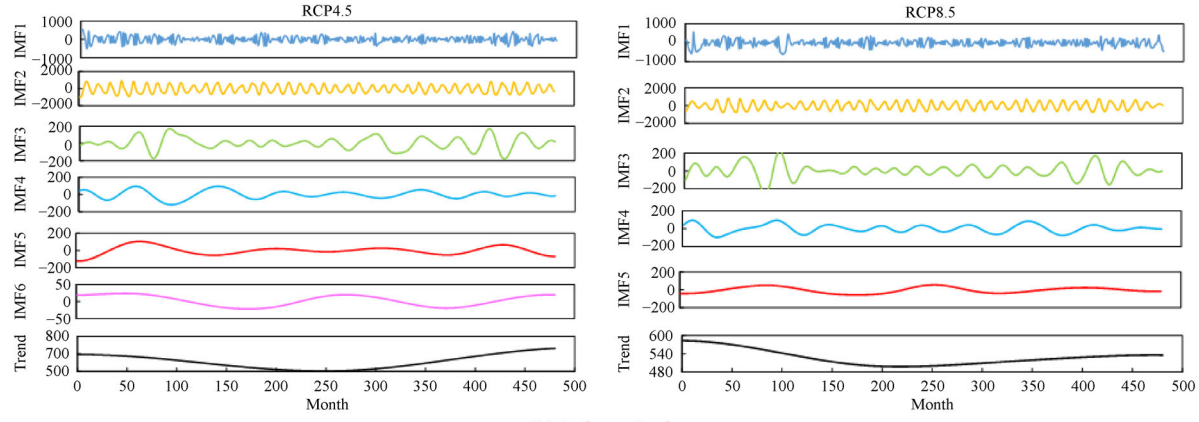

(b) Ankang Station

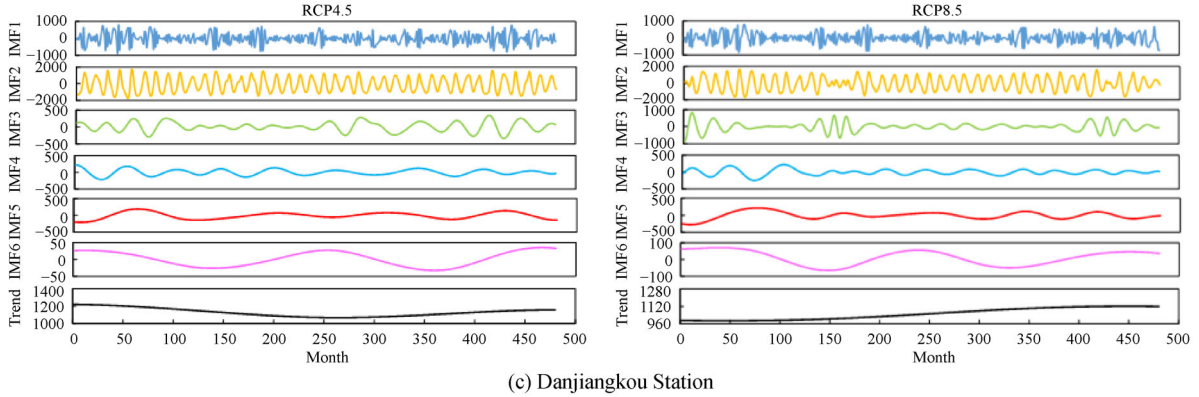

(c) Danjiangkou Station

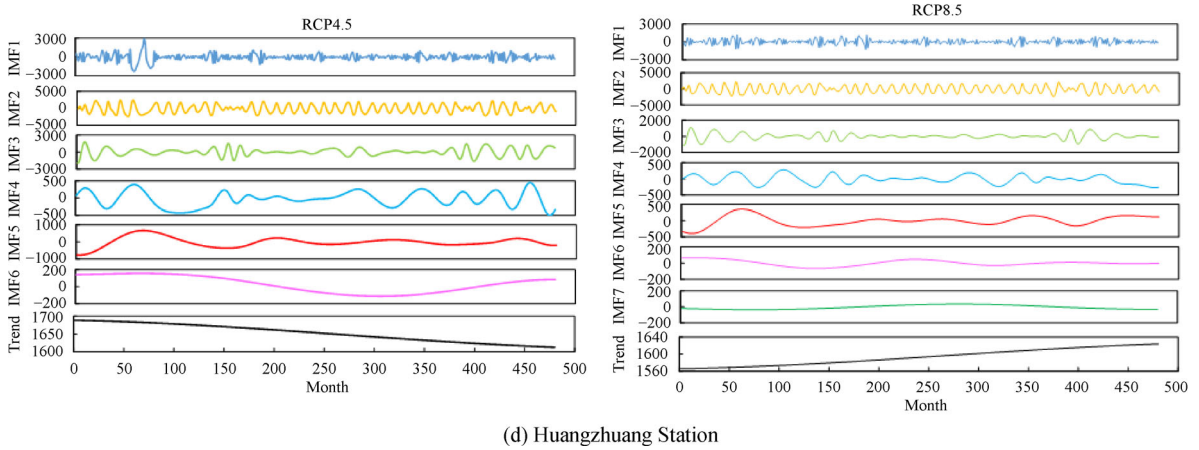

(d) Huangzhuang Station

Fig. 13 Decomposition of HDSI standard index series at four stations based on future monthly runoff.

based on the monthly runoff. Therefore, the monthly runoff is the most basic data of future runoff, and its cycle plays a leading role.

5.3 Contribution of future runoff attributed to future climate change and LUCC

The individual contribution rate of mean runoff attributed to future climate and LUCC in Han River basin is analyzed. The GCM ensemble median for mean is used to reduce the uncertainty in GCMs. The results of climate and LUCC contribution rate of the four hydrological stations at annual scale are shown in Table 7.

For the driving factors (Table 7), we find following characteristics. 1) The annual contribution rate of climate change to runoff at Baihe, Ankang, Danjiangkou, and Huangzhuang stations under RCP4.5 (RCP8.5), are 90.70% (83.69%), 91.90% (79.97%), 92.88% (84.76%), and 97.95% (94.17%), respectively. While the contribution rate of LUCC to runoff at the four stations under RCP4.5 (RCP8.5) are 2%–9% (6%–16%) on the annual scale. The results show that the mean annual runoff in the future are projected to increase under climate change alone or LUCC alone. 2) Climate change plays a more critical role in future runoff compared with LUCC in the Han River basin. The decisive effect of future climate change found in this study is consistent with Pan et al. (2017). 3) The combined impact is larger than that of individual impact, but is not equal to the sum of the two individual impacts. This is due to the complex interaction between climate change and LUCC, and the impact on runoff is not a direct linear superposition. 4) What's more, the contribution rate of LUCC to four hydrological stations is different, which is due to the spatial heterogeneity caused by LUCC.

6 Conclusions

In this study, we developed a framework to assess the runoff variation response to single or combined future climate change and LUCC. First, the DBC method and CA-Markov model are applied to project future climate and LUCC scenarios, respectively. Then the SWAT model is used to simulate and project the response of runoff under designed scenarios. Finally, future runoff is analyzed by variation assessment, uncertainty, and characteristics analysis, contribution attributed to future climate change and LUCC. The main conclusions are as follows.

1) Both climate change and LUCC will lead to an increase in runoff, the variation of future runoff under combined climate and LUCC is larger than that under climate change or LUCC alone.

2) Future runoff response under ten GCMs at Baihe, Ankang, Danjiangkou, and Huangzhuang stations are all of high uncertainty, the projected uncertainty of median value of multi-models under RCP4.5 (RCP8.5) will reach 18.14% (20.34%), 12.18% (14.71%), 11.01% (13.95%), and 11.41% (14.34%), respectively.

3) The contribution rate of climate change to runoff at Baihe, Ankang, Danjiangkou, and Huangzhuang stations under RCP4.5 (RCP8.5) are 91%–98% (84%–94%), while LUCC to runoff under RCP4.5 (RCP8.5) only accounts for 2%–9% (6%–16%) in the annual scale.

This study will help to maintain the water resources

Table 6 Average period of IMF of four hydrological stations in the Han River (month)

Scenarios	Stations	IMF1	IMF2	IMF3	IMF4	IMF5	IMF6	IMF7
RCP4.5	Baihe	2.99	6.51	14.35	24.79	61.21	121.75	234.35
	Ankang	2.84	6.50	16.87	30.91	60.09	120.08	/
	Danjiangkou	2.77	6.49	16.52	27.54	60.25	118.76	/
	Huangzhuang	2.83	6.10	11.60	26.30	60.09	236.66	/
RCP8.5	Baihe	2.85	6.24	11.52	19.06	48.32	81.17	/
	Ankang	2.94	6.53	12.79	29.98	79.00	/	/
	Danjiangkou	2.68	6.12	11.81	20.14	46.80	116.32	/
	Huangzhuang	2.71	6.26	12.01	20.70	48.97	103.97	120.02

Table 7 Annual contribution rate of future climate change and LUCC at four stations (%)

Scenarios	Stations	Baihe	Ankang	Danjiangkou	Huangzhuang
RCP4.5	Climate change	90.70	91.90	92.88	97.95
	LUCC	9.30	8.10	7.12	2.05
	Total	100.00	100.00	100.00	100.00
RCP8.5	Climate change	83.69	79.97	84.76	94.17
	LUCC	16.31	20.03	15.24	5.83
	Total	100.00	100.00	100.00	100.00

management and ecological environment protection planning and design of the Han River basin under the synthetic change of climate and LUCC in the future. In addition, the impacts of future climate change and LUCC on runoff may vary with basin changes due to different climatic characteristics. Moreover, the results may vary across different climate models, land use projection models, and hydrological models. Therefore, it is necessary to investigate these integrated uncertainties to provide a better understanding on future water resources management.

Acknowledgements This work was supported by the National Natural Science Foundation of China (Grant Nos. U20A20317 and 51539009). The authors would like to thank Mingxi Shen for his comments, and for the editor and anonymous reviewers that helped improve the quality of the paper.

References

Abbaspour K C, Yang J, Maximov I, Siber R, Bogner K, Mieleitner J, Zobrist J, Srinivasan R (2007). Modelling hydrology and water quality in the pre-alpine/alpine Thur watershed using SWAT. J Hydrol (Amst), 333(2–4): 413–430

Ahmadalipour A, Moradkhani H, Rana A (2018). Accounting for downscaling and model uncertainty in fine-resolution seasonal climate projections over the Columbia River Basin. Clim Dyn, 50(1–2): 717–733

Berihun M L, Tsunekawa A, Haregeweyn N, Meshesha D T, Adgo E, Tsubo M, Masunaga T, Fenta A A, Sultan D, Yibeltal M, Ebabu K (2019). Hydrological responses to land use/land cover change and climate variability in contrasting agro-ecological environments of the Upper Blue Nile basin, Ethiopia. Sci Total Environ, 689: 347–365

Block K, Mauritsen T (2013). Forcing and feedback in the MPI-ESM-LR coupled model under abruptly quadrupled CO_2. J Adv Model Earth Syst, 5(4): 676–691

Changnon D, Gensini V A (2019). Changing spatiotemporal patterns of 5- and 10-Day Illinois heavy precipitation amounts, 1900–2018. J Appl Meteorol Climatol, 58(7): 1523–1533

Chauvin F, Douville H, Ribes A (2017). Atlantic tropical cyclones water budget in observations and CNRM-CM5 model. Clim Dyn, 49(11–12): 4009–4021

Chawla I, Mujumdar P P (2015). Isolating the impacts of land use and climate change on streamflow. Hydrol Earth Syst Sci, 19(8): 3633–3651

Chen H, Guo S L, Xu C Y, Singh V P (2007). Historical temporal trends of hydro-climatic variables and runoff response to climate variability and their relevance in water resource management in the Hanjiang basin. J Hydrol (Amst), 344(3–4): 171–184

Chen J, Brissette F P, Chaumont D, Braun M (2013). Performance and uncertainty evaluation of empirical downscaling methods in quantifying the climate change impacts on hydrology over two North American river basins. J Hydrol (Amst), 479: 200–214

Clerici N, Cote-Navarro F, Escobedo F J, Rubiano K, Villegas J C (2019). Spatio-temporal and cumulative effects of land use-land cover and climate change on two ecosystem services in the Colombian Andes. Sci Total Environ, 685: 1181–1192

Costa M H, Botta A, Cardille J A (2003). Effects of large-scale changes in land cover on the discharge of the Tocantins River, Southeastern Amazonia. J Hydrol (Amst), 283(1–4): 206–217

da Silveira I, Zuidema P, Kirtman B P (2019). Fast SST error growth in the southeast Pacific Ocean: comparison between high and low-resolution CCSM4 retrospective forecasts. Clim Dyn, 53(9–10): 5237–5251

Frey L, Bender A M, Svensson G (2021). Processes controlling the vertical aerosol distribution in marine stratocumulus regions- a sensitivity study using the climate model NorESM1-M. Atmos Chem Phys, 21(1): 577–595

Gassman P W, Reyes M R, Green C H, Arnold J G (2007). The soil and water assessment tool: historical development, applications, and future research directions. Trans ASABE, 50(4): 1211–1250

Gu L, Chen J, Yin J B, Xu C-Y (2020). Responses of precipitation and runoff to climate warming and implications for future drought changes in China. Earth's Future, 8(10): e2020EF001718.

Guan D J, Li H F, Inohae T, Su W C, Nagaie T, Hokao K (2011). Modeling urban land use change by the integration of cellular automaton and Markov model. Ecol Modell, 222(20–22): 3761–3772

Guo Y, Fang G, Xu Y P, Tian X, Xie J (2020). Identifying how future climate and land use/cover changes impact streamflow in Xinanjiang Basin, East China. Sci Total Environ, 710: 136275

Halmy M W A, Gessler P E, Hicke J A, Salem B B (2015). Land use/land cover change detection and prediction in the north-western coastal desert of Egypt using Markov-CA. Appl Geogr, 63: 101–112

Huang N E, Shen Z, Long S R, Wu M C, Shih H H, Zheng Q, Yen N C, Tung C C, Liu H H (1998). The empirical mode decomposition and the Hilbert spectrum for nonlinear and non-stationary time series analysis. In: Proceedings Mathematical Physical & Engineering Conferences, 454: 903–995

Huang N E, Shen Z, Long S R (1999). A new view of nonlinear water waves: the Hilbert Spectrum 1. Annu Rev Fluid Mech, 31(1): 417–457

Hyandye C, Martz L W (2017). A Markovian and cellular automata land-use change predictive model of the Usangu Catchment. Int J Remote Sens, 38(1): 64–81

Ji D, Wang L, Feng J, Wu Q Z, Zhou M Z (2014). Description and basic evaluation of BNU-ESM version 1. Geoscientific Model Devel Discuss, 7(2): 1601–1647

Khazaei M R, Zahabiyoun B, Saghafian B (2012). Assessment of climate change impact on floods using weather generator and continuous rainfall-runoff model. Int J Climatol, 32(13): 1997–2006

Kundu S, Khare D, Mondal A (2017). Individual and combined impacts of future climate and land use changes on the water balance. Ecol Eng, 105: 42–57

Kusangaya S, Warburton M L, van Garderen E A, Jewitt G P W (2014). Impacts of climate change on water resources in southern Africa: a review. Phys Chem Earth, 67–69: 47–54

Li S S, Zhang L, Du Y, Zhang Y H, Yan C C (2020). Anthropogenic impacts on streamflow-compensated climate change effect in the Hanjiang River basin, China. J Hydrol Eng, 25(1): 04019058

Li Y, Chang J, Wang Y, Guo A, Luo L, Ma F, Fan J(2019). Spatiotemporal impacts of land use land cover changes on hydrology from the mechanism perspective using SWAT model with time-

varying parameters. Hydrol Res, 50(1): 244–261

Liang Z, Tang T, Li B, Liu T, Wang J, Hu Y (2018). Long-term streamflow forecasting using SWAT through the integration of the random forests precipitation generator: case study of Danjiangkou Reservoir. Hydrol Res, 49(5): 1513–1527

Lin B, Chen X, Yao H, Chen Y, Liu M, Gao L, James A (2015). Analyses of landuse change impacts on catchment runoff using different time indicators based on SWAT model. Ecol Indic, 58: 55–63

Luo G, Yin C, Chen X, Xu W, Lu L (2010). Combining system dynamic model and CLUE-S model to improve land use scenario analyses at regional scale: a case study of Sangong watershed in Xinjiang, China. Ecol Complex, 7(2): 198–207

Memarian H, Kumar Balasundram S, Bin Talib J, Teh Boon Sung C, Mohd Sood A, Abbaspour K (2012). Validation of CA-Markov for simulation of land use and cover change in the Langat Basin, Malaysia. J Geogr Inf Syst, 04(06): 542–554

Mishra S K, Pandey A, Singh V P (2012). Special issue on soil conservation service curve number (SCS-CN) methodology. J Hydrol Eng, 17(11): 1157

Mpelasoka F S, Chiew F H S (2009). Influence of rainfall scenario construction methods on runoff projections. J Hydrometeorol, 10(5): 1168–1183

Paymard P, Yaghoubi F, Nouri M, Bannayan M (2019). Projecting climate change impacts on rainfed wheat yield, water demand, and water use efficiency in northeast Iran. Theor Appl Climatol, 138(3–4): 1361–1373

Nouri J, Gharagozlou A, Arjmandi R, Faryadi S, Adl M (2014). Predicting urban land use changes using a CA-Markov Model. Arab J Sci Eng, 39(7): 5565–5573

Pan S H, Liu D D, Wang Z L, Zhao Q, Zou H, Hou Y K, Liu P, Xiong L H (2017). Runoff responses to climate and land use/cover changes under future scenarios. Water, 9(7): 475

Pontius R G Jr, Neeti N (2010). Uncertainty in the difference between maps of future land change scenarios. Sustain Sci, 5(1): 39–50

Poska A, Sepp E, Veski S, Koppel K (2008). Using quantitative pollen-based land-cover estimations and a spatial CA-Markov model to reconstruct the development of cultural landscape at Ruge, South Estonia. Veg Hist Archaeobot, 17(5): 527–541

Richey A S, Thomas B F, Lo M H, Reager J T, Famiglietti J S, Voss K, Swenson S, Rodell M (2015). Quantifying renewable groundwater stress with GRACE. Water Resour Res, 51(7): 5217–5238

Schmidli J, Frei C, Vidale P L (2006). Downscaling from GC precipitation: a benchmark for dynamical and statistical downscaling methods. Int J Climatol, 26(5): 679–689

Schuol J, Abbaspour K C, Srinivasan R, Yang H (2008). Estimation of freshwater availability in the West African sub-continent using the SWAT hydrologic model. J Hydrol (Amst), 352(1–2): 30–49

Senroy N, Suryanarayanan S, Ribeiro P F (2007). An improved Hilbert–Huang method for analysis of time-varying waveforms in power quality. IEEE Trans Power Syst, 22(4): 1843–1850

Shen M X, Chen J, Zhuan M J, Chen H, Xu C Y, Xiong L H (2018). Estimating uncertainty and its temporal variation related to global climate models in quantifying climate change impacts on hydrology. J Hydrol (Amst), 556: 10–24

Shen J J, Yen W P, O'Fallon J (2003). Interpretation and application of Hilbert-Huang transformation for seismic performance analyses. In: 6th US Conference & Workshop on Lifeline Earthquake Engineering (TCLEE)

Tao F, Yokozawa M, Hayashi Y, Lin E (2003). Future climate change, the agricultural water cycle, and agricultural production in China. Agric Ecosyst Environ, 95(1): 203-215 2

Teng J, Vaze J, Chiew F H S, Wang B, Perraud J M (2012). Estimating the relative uncertainties sourced from GCMs and hydrological models in modeling climate change impact on runoff. J Hydrometeorol, 13(1): 122–139

Trolle D, Nielsen A, Andersen H E, Thodsen H, Olesen J E, Børgesen C D, Refsgaard J C, Sonnenborg T O, Karlsson I B, Christensen J P, Markager S, Jeppesen E (2019). Effects of changes in land use and climate on aquatic ecosystems: coupling of models and decomposition of uncertainties. Sci Total Environ, 657: 627–633

Umair M, Kim D, Choi M (2019). Impacts of land use/land cover on runoff and energy budgets in an East Asia ecosystem from remotely sensed data in a community land model. Sci Total Environ, 684: 641–656

Wagner P D, Kumar S, Schneider K (2013). An assessment of land use change impacts on the water resources of the Mula and Mutha Rivers catchment upstream of Pune, India. Hydrol Earth Syst Sci, 17(6): 2233–2246

Wang L, Guo S L, Hong X J, Liu D D, Xiong L H (2017). Projected hydrologic regime changes in the Poyang Lake Basin due to climate change. Front Earth Sci, 11(1): 95–113

Woldesenbet T A, Elagib N A, Ribbe L, Heinrich J (2018). Catchment response to climate and land use changes in the Upper Blue Nile sub-basins, Ethiopia. Sci Total Environ, 644: 193–206

Wu C H, Huang G R (2015). Changes in heavy precipitation and floods in the upstream of the Beijiang River basin, south China. Int J Climatol, 35(10): 2978–2992

Wu T (2012). A mass-flux cumulus parameterization scheme for large-scale models: description and test with observations. Clim Dyn, 38(3–4): 725–744

Wu Z H, Huang N E (2004). A study of the characteristics of white noise using the empirical mode decomposition method. Proc Royal Soc, Math Phys Eng Sci, 460(2046): 1597–1611

Yan L, Xiong L H, Liu D D, Hu T S, Xu C Y (2017). Frequency analysis of nonstationary annual maximum flood series using the time-varying two-component mixture distributions. Hydrol Processes, 31(1): 69–89

Yin J, He F, Xiong Y J, Qiu G Y (2017). Effects of land use/land cover and climate changes on surface runoff in a semi-humid and semi-arid transition zone in northwest China. Hydrol Earth Syst Sci, 21(1): 183–196

Yin J, Gentine P, Zhou S, Sullivan S C, Wang R, Zhang Y, Guo S (2018). Large increase in global storm runoff extremes driven by climate and anthropogenic changes. Nat Commun, 9(1): 4389

Yu B, Li G, Chen S, Lin H (2020). The role of internal variability in climate change projections of North American surface air temperature and temperature extremes in CanESM2 large ensemble simulations. Clim Dyn, 55(3–4): 869–885

Zhang D F, Han Z Y, Shi Y (2017). Comparison of climate projections between driving CSIRO-Mk3.6.0 and downscaling simulation of RegCM4.4 over China. Adv Clim Change Res, 8(4): 245–255

Zhang H, Huang G H, Wang D, Zhang X (2011). Uncertainty assessment of climate change impacts on the hydrology of small prairie wetlands. J Hydrol (Amst), 396(1–2): 94–103

Zhang L, Nan Z, Yu W, Ge Y (2016a). Hydrological responses to land-use change scenarios under constant and changed climatic conditions. Environ Manage, 57(2): 412–431

Zhang L, Chen X L, Lu J Z, Fu X K, Zhang Y F, Liang D, Xu Q Q (2019). Precipitation projections using a spatiotemporally distributed method: a case study in the Poyang Lake watershed based on the MRI-CGCM3. Hydrol Earth Syst Sci, 23(3): 1649–1666

Zhang Q, Liu J Y, Singh V P, Gu X H, Chen X H (2016b). Evaluation of impacts of climate change and human activities on streamflow in the Poyang Lake basin, China. Hydrol Processes, 30(14): 2562–2576

Zhao M M, He Z B, Du J, Chen L F, Lin P F, Fang S (2019). Assessing the effects of ecological engineering on carbon storage by linking the CA-Markov and InVEST models. Ecol Indic, 98: 29–38

Zhou F, Xu Y, Chen Y, Xu C Y, Gao Y, Du J (2013). Hydrological response to urbanization at different spatio-temporal scales simulated by coupling of CLUE-S and the SWAT model in the Yangtze River Delta region. J Hydrol (Amst), 485: 113–125

Zuo D, Xu Z, Yao W, Jin S, Xiao P, Ran D (2016). Assessing the effects of changes in land use and climate on runoff and sediment yields from a watershed in the Loess Plateau of China. Sci Total Environ, 544: 238–250